1993ApJ...416..496C

THE ASTROPHYSICAL JOURNAL, 416:496–518, 1993 October 20
© 1993. The American Astronomical Society. All rights reserved. Printed in U.S.A.

MILLIARCSECOND POLARIZATION STRUCTURE OF 24 OBJECTS FROM THE PEARSON-READHEAD SAMPLE OF BRIGHT EXTRAGALACTIC RADIO SOURCES. I. THE IMAGES

T. V. CAWTHORNE,[1,2,3] J. F. C. WARDLE,[1] D. H. ROBERTS,[1] D. C. GABUZDA,[4] AND L. F. BROWN[1,5]
Received 1992 September 1; accepted 1993 April 27

ABSTRACT

This paper presents the first survey of the milliarcsecond-scale linear polarization properties of compact extragalactic radio sources. Global VLBI observations in total intensity and linear polarization at a frequency of 5 GHz (λ6 cm) of 24 sources from the Pearson-Readhead complete sample are presented. We have observed 12 quasars, eight BL Lacertae objects, and four galaxies, constituting about half of the Pearson-Readhead list. We show total intensity and polarization images of all 16 sources in which we detected significant polarized flux on milliarcsecond scales, and total intensity images of two additional sources. The properties of the individual sources are discussed at some length. A detailed analysis of the sample is given in an accompanying paper.

Subject headings: BL Lacertae objects: general — polarization — quasars: general — surveys — techniques: interferometric

1. INTRODUCTION

This paper represents the first determination of the linear polarization characteristics of a large, representative sample of extragalactic radio sources on milliarcsecond scales. The sources observed are taken from the sample defined by Pearson & Readhead (1984, 1988), nearly all of which have been mapped in total intensity by those authors.

The importance of linear polarization measurements as a diagnostic of emission mechanisms, relativistic and thermal particle populations, and magnetic fields in extragalactic radio sources is well known. On arcsecond scales polarization studies have greatly increased our understanding of the physical properties of jets, lobes, and hot spots (see, for example, Scheuer 1987). Polarization studies on the smaller scales accessible to VLBI can be expected to yield similar advances. Such observations should increase our understanding of the magnetic field structures and source environments of active galactic nuclei (AGNs), as well as that of the relationships among the different classes of radio sources.

Although many sources have been imaged in total intensity at milliarcseconds resolution using hybrid mapping techniques, it is only recently that observations at similar resolution have yielded polarization images. The techniques are described by Roberts et al. (1984), Wardle & Roberts (1986), Roberts, Brown, & Wardle (1991), and Roberts, Wardle, & Brown (1993). Polarization images published to date include those of the superluminal quasars 3C 273 (Roberts et al. 1990a) and 3C 345 (Wardle et al. 1986, 1988; Brown, Roberts, & Wardle 1993) and of a large number of BL Lacertae objects (Roberts, Gabuzda, & Wardle 1987; Gabuzda, Wardle, & Roberts 1989b; Gabuzda et al. 1989a, 1992, hereafter GCRW89a and GCRW92). Here we present the first results of our survey of the polarization properties of a large and representative sample of compact radio sources selected only according to the brightness of compact features. Part of the motivation for this work is to overcome any prejudices that may arise as a result of focusing attention on famous sources such as 3C 273. Preliminary results based in part on this survey were presented by Roberts et al. (1990b).

The observational program is based upon the sample defined by Pearson & Readhead (1984, 1988), which consists of 65 sources brighter than 1 Jy at 5 GHz (λ6 cm). Of the 65 sources, 46 show fringes on long baselines, and most of this subsample have been imaged in total intensity at one or more epochs by the Caltech group. So far, 34 of these 46 sources have been observed as part of the Brandeis polarization program. Of the remaining 12 sources, eight are very weakly polarized and are unlikely to be a high priority for this type of observation. The remaining four will be observed in the near future. This paper presents the results for 24 of the 34 sources observed to date. The sources that have been observed but are not discussed here include 3C 236, which showed no detectable fringes on the longer baselines, and nine sources from recent experiments, presently in various stages of correlation or calibration.

Of the 24 sources discussed in this paper, total intensity and linear polarization images are presented for those 16 sources that exhibit detectable polarized flux on milliarcsecond scales. The eight sources that are unpolarized include all four galaxies and two quasars that were found also to be unpolarized at VLA resolution. VLBI total intensity images of these sources made from observations with better u-v coverage than ours have appeared elsewhere. For completeness, we discuss these eight sources in § 3 and include them in the tables of results, but we do not show images of them. Two BL Lacertae objects were found to be polarized at the VLA, but not at VLBI resolution. Their polarized emission must reside on subarcsecond scales larger than those probed by the present obser-

[1] Department of Physics, Brandeis University, Waltham, MA 02254; Internet:vlbi@binah.cc.brandeis.edu.
[2] Harvard-Smithsonian Center for Astrophysics, 60 Garden Street, Cambridge, MA 02138.
[3] Present address: Department of Physics and Astronomy, University of Central Lancashire, Preston PR1 2HE, Lancashire, UK.
[4] Department of Physics and Astronomy, University of Calgary, Calgary, Alberta, Canada T2N 1N4.
[5] Present address: Department of Physics and Astronomy, Connecticut College, New London, CT 06320.

© American Astronomical Society • Provided by the NASA Astrophysics Data System

1993ApJ...416..496C

vations. Total intensity images of these two sources are presented by GCRW92 and are also reproduced here.

A complete list of the Pearson-Readhead sources is given in Table 1. There we show the IAU name in column (1), alias in column (2), optical identification in column (3), redshift in column (4), epochs at which we have taken VLBI polarization data in column (5), and the classification of the total intensity structure in column (6) as given by Pearson & Readhead (1988, hereafter PR88). For definitions of the structural categories the reader is referred to their paper.

Section 2 briefly describes the observations. Section 3 presents the results of these observations source by source. The structures are discussed in the light of other recent (total intensity) VLBI work. A detailed discussion of the polarization

TABLE 1

THE PEARSON-READHEAD SAMPLE

Source (IAU) (1)	Alias (2)	Optical ID (3)	Redshift (4)	Epochs (5)	*I* Structure (6)
0016+731	...	Q	1.781	1984 Oct[b]	Very compact
0108+388	...	G	0.669	1984 Mar[b]	Compact S double
0133+476	OC 457	Q	0.859	1984 Mar[b]	Compact
0153+744	...	Q	2.338	1984 Mar[b]	Compact F double
0212+735	...	Q	2.367	1984 Mar[b]	Asymmetric I
0316+413	3C 84	G	0.0172	Many	Irregular
0404+768	...	G	...	...	Steep-spectrum compact
0454+844	...	B	...	1984 Oct,[b,c] 1989 Apr[d]	Asymmetric I
0538+498	3C 147	Q	0.545	...	Steep-spectrum compact
0710+439	OI 417	G	0.518	...	Compact S double
0711+356	OI 318	Q	1.62	1984 Mar[b]	Compact F double
0723+679	3C 179	Q	0.846	...	Nucleus of FR II
0804+449	OJ 508	Q	1.43	1990 Jun[d]	Very compact
0814+425	OJ 425	Q	...	...	Compact
0831+557	4C 55.16	G	0.242	...	Irregular
0836+710	4C 71.07	Q	2.17	1984 Mar[b]	Asymmetric II
0850+581	4C 58.17	Q	1.322	...	Compact
0859+470	4C 47.29	Q	1.462	...	Asymmetric I
0906+430	3C 216	Q	0.67	1990 Jun[d]	Steep-spectrum compact
0923+392	4C 39.25	Q	0.699	...	Compact F double
0945+408	4C 40.24	Q	1.252	...	Asymmetric II
0954+556	4C 55.17	Q	0.909	...	(Not observed by PR)
0954+658	...	B	0.368	1987 May,[b,e] 1989 Apr[d]	(Not observed by PR)
1003+351	3C 236	G	0.0989	...	Nucleus of FR II
1031+567	OL 553	G	0.45	...	(Not observed by PR)
1358+624	4C 66.22	G	0.431	...	(Not observed by PR)
1458+718	3C 309.1	Q	0.905	1988 Nov[d]	Steep-spectrum compact
1624+416	4C 31.32	Q	2.55	1984 Oct[b]	Asymmetric II
1633+382	4C 38.41	Q	1.814	1984 Oct[b]	Asymmetric II
1637+574	OS 562	Q	0.745	1988 Nov[d]	Very compact
1641+399	3C 345	Q	0.595	Many[f]	Asymmetric II
1642+690	4C 69.21	Q	0.751	...	Compact
1652+398	4C 39.49	B	0.0337	1987 May,[b,c] 1989 Apr[d]	Asymmetric II
1739+522	4C 51.37	Q	1.375	1988 Jun[d]	Very compact
1749+701	...	B	0.770	1989 Apr[d]	Asymmetric
1803+784	...	B	0.68	1987 May,[b,e] 1989 Apr[d]	Asymmetric I
1807+698	3C 371	B	0.050	1984 Mar[b,c]	Asymmetric II
1823+568	4C 56.27	B	0.664	1984 Oct[b,c]	Asymmetric I
1828+487	3C 380	Q	0.692	1984 Oct[b]	Steep-spectrum compact
1845+797	3C 390.3	G	0.0569	...	Nucleus of FR II
1928+738	4C 73.18	Q	0.302	1984 Mar[b]	Asymmetric I
1954+513	OV 591	Q	1.22	...	Asymmetric I
2021+614	OW 637	G	0.2266	1984 Mar[b]	Compact F double
2200+420	BL Lac	B	0.07	1984 Mar,[c] 1984 Oct[b]	Asymmetric I
2351+456	4C 45.51	Q	2.0	1984 Oct[b]	Asymmetric II
2352+495	OZ 488	G	0.237	1984 Oct[b]	Compact S double

[a] Excluding sources not detected in the fringe finding survey.
[b] This paper
[c] Gabuzda et al. 1989a.
[d] Reduction in progress.
[e] Gabuzda, et al. 1992.
[f] Brown, Roberts, & Wardle 1993.

© American Astronomical Society • Provided by the NASA Astrophysics Data System

1993ApJ...416..496C

TABLE 2

OBSERVING LOG

Date	Epoch	Antennas	Mark III Mode	Frequency (MHz)	Bandwidth[a] (MHz)
1984 March	1984.23	$BKGFY_{27}O$	A	4987	28
1984 October	1984.77	$BKGFY_{27}O$	A	4987	28
1987 May	1987.41	$LBW_{14}KGFY_{27}O$	C	4984	14

[a] Bandwidth per polarization.

properties of the whole sample, and of the striking differences as a function of optical identification, is given in the accompanying paper (Cawthorne et al. 1993, hereafter Paper II).

2. OBSERVATIONS

The observations presented here were made during three observing sessions in 1984 and 1987 (see Table 2) using global VLBI arrays. The properties of the antennas are listed in Table 3. In all cases the observing frequency was 5 GHz. Both left and right circularly polarized signals were recorded at all stations (except at Bonn in 1987, where only left circular polarization was recorded) using the Mark III system. The 1984 observations used a 28 MHz bandwidth in each polarization; the 1987 observations used a 14 MHz bandwidth but longer scans, so the sensitivities of the three observing sessions are comparable. The last column of Table 3 lists the average instrumental polarization amplitude of each antenna, averaged over both polarizations and all epochs. The data were correlated on the Haystack Mark III correlator. Calibration and imaging were then performed as described by Roberts et al. (1984), Wardle & Roberts (1986), Roberts et al. (1991), and Roberts et al. (1993).

It is important to note that these observations are part of a survey rather than detailed investigations of individual sources. Typically, each source was observed at only six to eight hour angles. Together with the modest number of antennas (especially in the first two sessions), such observations constitute a "snapshot" rather than a full synthesis. After editing and with the occasional instrumental failure, some sources have particularly sparse u-v coverage, and extended features may be very undersampled. For the most part, our total intensity images are in good agreement with those previously published. In a few cases our results are clearly inferior and we defer to the earlier work. We believe that the primary features we detect and their polarization are correctly represented in our images. The faintest features may not be reliable. These considerations also affect the component flux and polarization values listed in Table 4. In most cases we have not attempted to derive component angular sizes, since we do not consider the u-v coverage adequate to yield meaningful diameters.

TABLE 3

ANTENNA PROPERTIES

Station	Code	Diameter (m)	T_{sys} (Jy)	$\langle \lvert D \rvert \rangle$[a]
Medicina	L	32	300	0.160
Effelsberg.....	B	100	50	0.054
Westerbork	W_{14}	14 × 25[b]	70	0.094
Haystack	K	37	440	0.020
Green Bank	G	43	200	0.081
Fort Davis	F	25	760	0.016
VLA	Y_{27}	27 × 25[b]	25	0.020
Owens Valley	O	40	200	0.010

[a] Mean cross-polarization response as a fraction of the total intensity.

[b] Phased array.

The overall accuracy of calibration of the flux density scale is about 10%. The instrumental polarization terms for each antenna have been determined to better than 0.5%. A detailed discussion of the errors in calibrating the polarized fringes and their effect on the polarized images will be presented in Roberts et al. (1993), where we conclude that the "lowest reliable P contour" is about 0.1% of the peak I intensity over most of the P image, and a factor of about 3 worse within a few beamwidths of the image center.

For all sources, the total flux in the VLBI image is less than the flux in the unresolved core measured simultaneously at the VLA, indicating structure on scales between a few tens of milliarcseconds and about 1 arcsecond. We can also subtract (vectorially) the sum of the clean components in the P image from the integrated polarization of the core measured at the VLA, and hence determine the polarization of this "intermediate-scale" structure (see Table 5). Subtracting vectors measured in very different ways is of course hazardous, but we believe that values of intermediate-scale polarized flux $P_{int} \gtrsim 25$ mJy are reliable. There are eight sources in this category, and they are interesting because we can determine whether alignments between polarization and structure found on milliarcsecond scales continue to larger distances from the core.

In the following section, the total intensity and linear polarization images of 18 sources are shown in Figures 1–18. In each case, the first panel of the figure shows the total intensity, displayed as contours of I. The second panel of each figure displays the linear polarization as contours of polarized intensity p, with tick marks indicating the position angles χ of the electric field.[6] In the third panel of each figure the linear polarization image (*heavy lines*) is superposed on the total intensity image (*light lines*), showing directly the relationship of the I and P structures. Our method of phase-calibrating the cross-polarized data ensures that the I and P images are registered to within a small fraction of a beamwidth (Roberts et al. 1993). Rotation measure corrections have been applied to the polarized images of all sources. Simultaneous multiwavelength VLBI polarization observations are needed to determine whether there are spatial variations in rotation measure on milliarcsecond scales (such observations are underway). In the absence of this information, we have used published rotation measures determined by wide-bandwidth L-band observations

[6] In our notation the linear polarization is represented by the complex quantity $P = Q + iU = pe^{2i\chi} = mIe^{2i\chi}$, where $p = (Q^2 + U^2)^{1/2} = mI$ is the polarized intensity, m is the fractional linear polarization, and χ is the position angle of the electric field vector, measured east from north.

© American Astronomical Society • Provided by the NASA Astrophysics Data System

1993ApJ...416..496C

TABLE 4

COMPONENT POSITIONS AND FLUXES

Source (IAU)	Component	x (mas)	y (mas)	r (mas)	θ (deg)	I (mJy)	p (mJy)	χ_{obs}[a] (deg)	RM (rad m^{-2})	m (%)	χ_{corr}[b] (deg)	Method
0016+731	N	0.0	0.0	...	...	802	14	56	-3 ± 11[c]	1.7	57	*u-v* fit
	SE	0.5	−0.2	0.5	112	171	<6	...		<3.5	...	
	S	−0.1	−2.1	2.1	−177	73	<4	...		<5.5	...	
0108+388[d]	...	...	...	...	...	...	...	...	...	...	...	...
0133+476	SE	0.0	0.0	...	...	800	14	135	109 ± 3[c]	1.8	112	*u-v* fit
	NW	−1.1	0.7	1.3	−58	213	<3	...		<1.4	...	
0153+744[d]	...	...	...	...	...	...	...	...	...	...	...	...
0212+735	Core	0.0	0.0	...	...	1081	9	25	14 ± 4[c]	0.8	22	*u-v* fit
	K4	1.1	−0.3	1.1	105	331	24	46		7.3	43	
	K3	2.1	−0.5	2.2	103	112	<5	...		<4.5	...	
	K2	5.5	−1.0	5.6	100	50	<5	...		<10.0	...	
	K1	13.2	0.3	13.2	91	62	12	42		19.4	39	
0316+413[d]	...	...	...	...	...	...	...	...	...	...	...	...
0454+844	NW	0.0	0.0	...	...	377	10	177	5 ± 6[c]	2.7	176	*u-v* fit
	SE	0.6	−1.1	1.3	151	137	12	162		8.8	161	
0711+356	S	0.0	0.0	...	...	230	<6	...	51 ± 13[c]	<2.6	...	Sum cc
	N	−1.7	4.5	4.8	−21	520	13	127		2.5	116	
0836+710	Core	0.0	0.0	...	...	600	<5	...	-9 ± 3[c]	<0.8	...	Sum cc
	K4	−0.4	−0.7	0.8	−150	150	<5	...		<3.3	...	
	K3	−1.4	−2.2	2.5	−145	260	31	94		11.9	96	
	K2	−4.9	−7.0	8.5	−145	260	34	80		13.1	82	
	K1	−5.5	−10.8	12.1	−153	16	11	115		69.0	117	
0954+658	Core	0.0	0.0	...	...	477	45	160	-15 ± 4[c]	9.4	163	*u-v* fit
	K3	−0.2	0.4	0.4	−27	218	<5	...		<2.3	...	
	K2	−1.1	0.4	1.1	−71	57	10	75		17.5	78	
	K1	−2.0	1.0	2.2	−65	32	<5	...		<15.6	...	
1624+416[d]	...	...	...	...	...	...	...	...	...	...	...	...
1633+382	Core	0.0	0.0	...	...	2285	34	31	4 ± 4[c]	1.5	33	*u-v* fit
	NW	−0.9	0.9	1.3	−45	148	<7	...		<4.7	...	
	SW	−2.2	−0.2	2.2	−95	104	<4	...		<3.8	...	
1641+399	D	0.0	0.0	...	...	2760	55	105	26 ± 8[c]	2.0	100	*u-v* fit
	C4	−0.7	0.0	0.7	−90	5580	197	161		3.5	156	
	C3	−2.8	0.6	2.9	−78	1030	104	27		10.1	22	
	C2	−5.8	2.0	6.1	−72	950	77	62		8.1	57	
1652+398	Core	0.0	0.0	...	...	457	<6	...	42[c]	<1.3	...	*u-v* fit
	K2	0.7	−0.9	1.1	142	162	<6	...		<3.7	...	
	K1	2.2	−2.0	3.0	132	118	<6	...		<5.1	...	
1749+701	Core	0.0	0.0	...	...	218	<4	...	10 ± 2[e]	<1.8	...	*u-v* fit
	K3	−0.7	0.4	0.8	−60	134	<4	...		<3.0	...	
	K2	−1.8	0.8	1.9	−67	45	<4	...		<8.9	...	
	K1	−2.7	2.1	3.4	−53	103	<4	...		<3.9	...	
1803+784	Core	0.0	0.0	...	...	1436	58	85	-70 ± 5[c]	4.0	100	*u-v* fit
	K2	−1.0	−0.1	1.0	−96	404	13	58		3.2	73	
	K1	−1.8	−0.3	1.8	−103	112	<2	...		<1.8	...	
1807+698[d]	Core	0.0	0.0	...	...	750	<4	...	339 ± 24[f]	<0.5	...	Sum cc
	Jet	...	...	~7	−97	240	7	4		2.9[d]	114[d]	
1823+568	Core	0.0	0.0	...	...	746	37	37	33 ± 2[e]	5.0	30	*u-v* fit
	K2	−0.2	−0.8	0.8	−166	101	12	26		12.0	19	
	K1	−0.5	−1.8	1.9	−165	58	5	23		8.6	16	
1828+487	Core	0.0	0.0	...	...	696	<4	...	130 ± 5[g]	<0.6	...	Sum cc
	K3	−3.2	5.3	6.2	−31	232	9	39		3.9	12	
	K2	−9.6	8.0	12.5	−50	65	50	43		77.0	16	
	K1	−14.3	9.5	17.2	−56	360	17	~40		4.7	~13	
1928+738	Core	0.0	0.0	...	...	1180	10	33	31 ± 1[e]	0.8	27	Sum cc
	K4	0.2	−2.2	2.2	175	300	25	35		8.3	29	
	K3	1.0	−4.2	4.3	167	240	24	68		10.0	62	
	K2	2.0	−9.0	9.2	168	176	31[d]	94[d]		~10[d]	88[d]	
	K1	3.0	−11.5	11.9	165	140						

© American Astronomical Society • Provided by the NASA Astrophysics Data System

1993ApJ...416..496C

TABLE 4—*Continued*

Source (IAU)	Component	x (mas)	y (mas)	r (mas)	θ (deg)	I (mJy)	p (mJy)	χ_{obs}[a] (deg)	RM (rad m^{-2})	m (%)	χ_{corr}[b] (deg)	Method
2021+614[d]	...	...	...	...	...	...	...	...	...	...	...	...
2200+420	Core	0.0	0.0	...	...	320	30	134	-205 ± 5[h]	9.4	176	*u-v* fit
	K3	−0.1	−1.3	1.3	−176	1260	70	142		5.6	4	
	K2	0.0	−2.7	2.7	−179	780	<7	...		<0.9	...	
	K1	0.8	−5.3	5.4	171	230	12	117		5.2	159	
2351+456	Core	0.0	0.0	...	...	580	7	68		1.2	(68)	Sum cc
	K1	−3.5	1.2	3.7	−71	250	19	88		7.6	(88)	
2352+495[d]	...	...	...	...	...	...	...	...	...	...	...	...

[a] Observed polarization position angles.
[b] Polarization position angles, corrected for Faraday rotation.
[c] Rusk 1988.
[d] See notes in § 3
[e] Wrobel et al. 1988.
[f] O'Dea 1989.
[g] Wilkinson et al. 1991.
[h] Rudnick et al. 1984.

at the VLA. The value we have used for each source and its reference are given in Table 4. A discussion of the possible hazards of using these data is given in Paper II.

3. RESULTS FOR INDIVIDUAL SOURCES

In this section we present the results of observations of 24 sources from the Pearson-Readhead sample. Table 4 lists component fluxes and polarizations. These are mostly derived from I and P model fitting to the phase-calibrated visibilities produced by the hybrid mapping process (GCRW89). In cases of clearly extended or diffuse components, or weak components that are poorly constrained by the model-fitting program, they are derived by summing the clean components (cc) within appropriately chosen boxes. We have not quoted errors on the component values listed in Table 4, because a major source of uncertainty lies not in the noise or calibration errors but in the fidelity of the images due to the limited *u-v* coverage. This varies from source to source and from component to component, and we have not found a satisfactory way to evaluate this. In general, values quoted for bright, barely resolved features should have errors of about 10% in I, and about 0.1–0.2 beamwidths in position. The error σ_p in polarized flux p is best judged from the lowest contour on the P image. The error in polarization position angle is then $\sigma_\chi \simeq \frac{1}{2} \arctan(\sigma_p/p)$ radians. We list both the observed polarization position angles and the position angles corrected for Faraday rotation, using the listed rotation measures. (Except for 2200+420 (BL Lac), for which the rotation measure is well established, these corrections are

TABLE 5

VLBI TO VLA SOURCE VISIBILITIES

Source	I_{VLBI} (mJy)	I_{VLA} (mJy)	γ_I	p_{VLBI} (mJy)	χ_{VLBI} (deg)	p_{VLA} (mJy)	χ_{VLA} (deg)	γ_p	p_{int} (mJy)	χ_{int} (deg)
0016+731	950	1190	0.80	14	58	19	60	0.74	<10	...
0108+388	1100	1200	0.92	...	...	<5	...	...	...	...
0133+476	1010	1340	0.76	14	135	25	106	0.56	21	89
0153+744	1120	1490	0.75	...	...	<5	...	...	...	...
0212+735	1690	2330	0.73	39	37	60	40	0.65	22	45
0316+413	58000	32000	0.55	...	...	<200	...	...	...	...
0454+844	510	630	0.81	19	170	24	162	0.79	<10	...
0711+356	800	885	0.90	13	127	14	106	0.93	10	74
0836+710	1580	2320	0.68	86	99	172	103	0.50	88	107
0954+658	730	890	0.82	36	159	47	164	0.77	13	178
1624+416	1040	1210	0.86	...	...	<3	...	...	...	...
1633+382	2610	2860	0.91	34	31	46	31	0.74	12	31
1641+399	10300	12500	0.82	202	21	287	25	0.70	103	53
1652+398	740	1360	0.54	<4	...	26	136	<0.15	26	136
1749+701	510	680	0.75	<5	...	14	110	<0.29	14	110
1803+784	1950	2480	0.79	64	89	96	79	0.67	42	63
1807+698	990	1690	0.59	7	4	40	54	0.18	42	59
1823+568	910	1280	0.71	52	37	56	37	0.93	<10	...
1828+487[a]	1120	2470	0.45	76	41	168	40	0.55	92	39
1928+738	2350	2760	0.85	69	74	78	93	0.88	49	123
2021+614	1910	2440	0.79	...	...	<5	...	...	...	...
2200+420	2590	3020	0.86	108	137	84	139	1.29	25	40
2351+456	910	1400	0.65	26	79	28	78	0.93	<10	...
2352+495	810	1580	0.51	...	...	<4	...	...	...	...

NOTE.—Values of χ are not corrected for Faraday rotation.
[a] VLA data taken from Rusk 1988 (not contemporaneous).

© American Astronomical Society • Provided by the NASA Astrophysics Data System

© American Astronomical Society • Provided by the NASA Astrophysics Data System

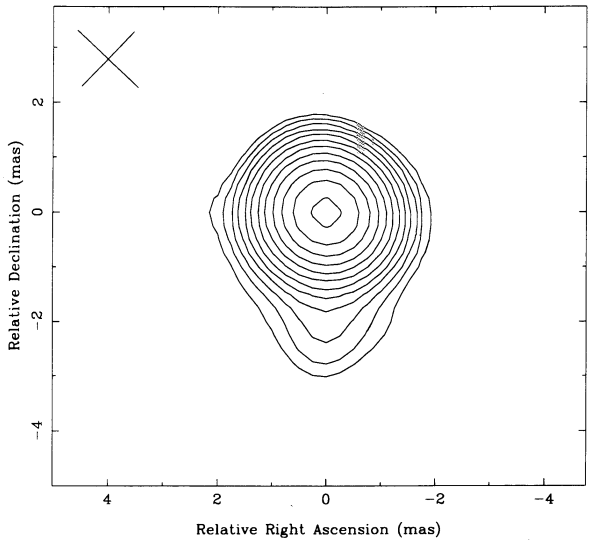

FIG. 1*a*

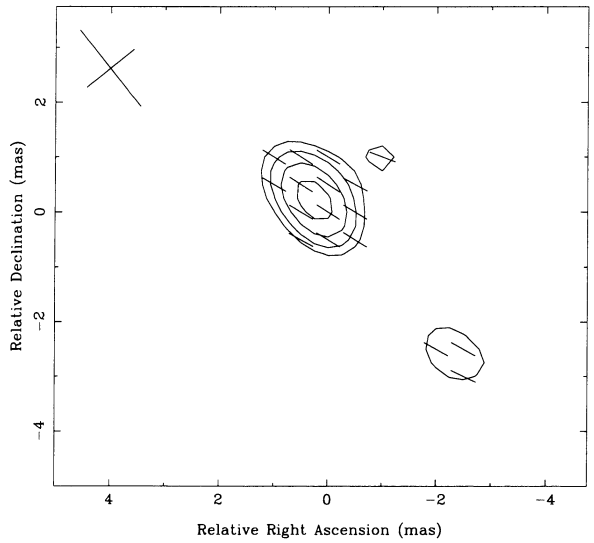

FIG. 1*b*

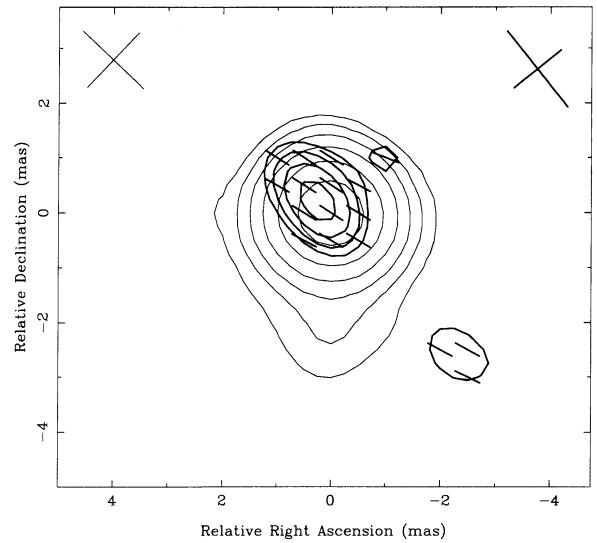

FIG. 1*c*

FIG. 1.—VLBI images of 0016+731 at 5 GHz, epoch 1984.78. (*a*) Total intensity, with contours at −2.0, 2.0, 2.8, 4.0, 5.7, 8.0, 11, 16, 22, 32, 45, 64, and 91% of the peak brightness of 921 mJy beam^{-1}. (*b*) Linear polarization, with contours of polarized intensity at 30, 42, 60, and 85% of the peak brightness of 13.2 mJy beam^{-1}, and sticks showing the orientations χ of the electric vectors (corrected for a rotation measure of −3 rad m^{-2}). (*c*) Superposition of the linear polarization image (*bold*) over the total intensity image, using only alternate *I* contours.

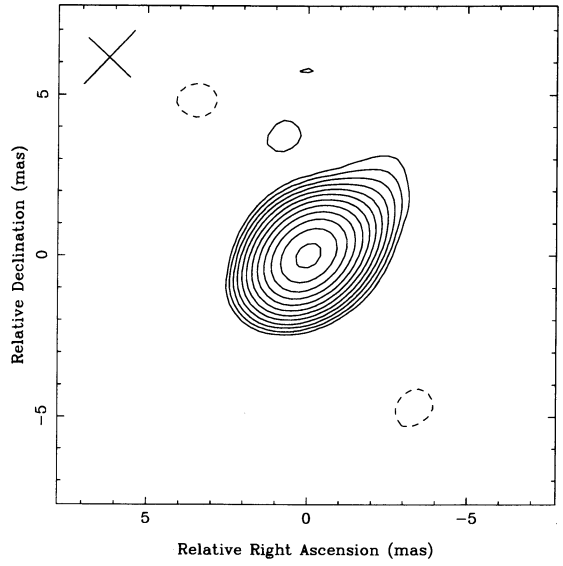

FIG. 2*a*

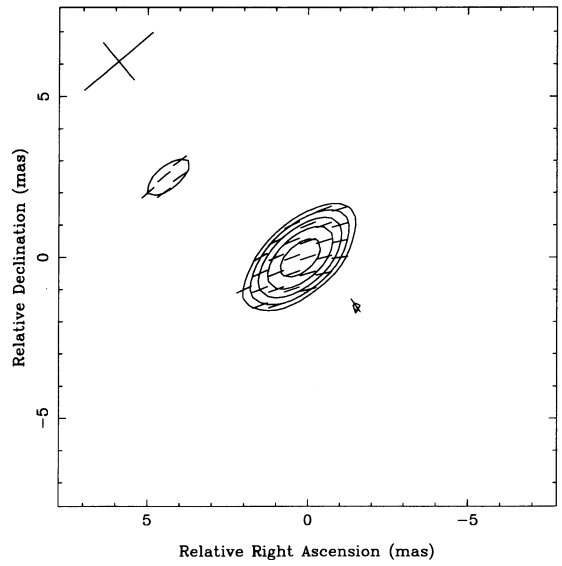

FIG. 2*b*

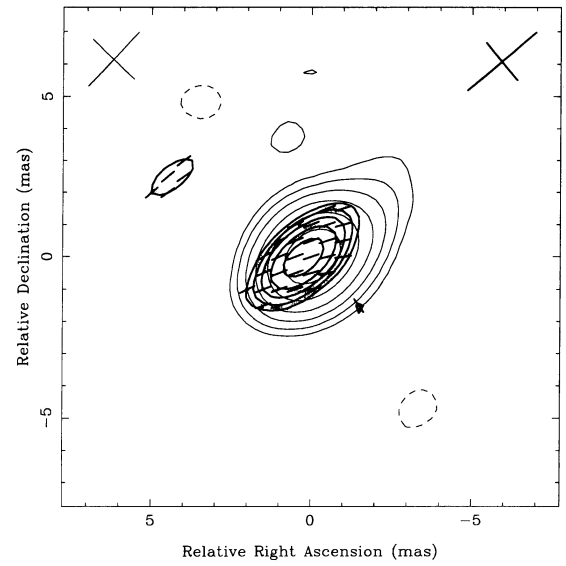

FIG. 2*c*

FIG. 2.—VLBI images of 0133+476 at 5 GHz, epoch 1984.23. (*a*) Total intensity, with contours at −2.0, 2.0, 2.8, 4.0, 5.7, 8.0, 11, 16, 22, 32, 45, 64, and 91% of the peak brightness of 903 mJy beam^{-1}. (*b*) Linear polarization, with contours of polarized intensity at 20, 28, 40, 57, and 80% of the peak brightness of 14.1 mJy beam^{-1}, and sticks showing the orientations χ of the electric vectors (corrected for a rotation measure of +109 rad m^{-2}). (*c*) Superposition of the linear polarization image (*bold*) over the total intensity image, using only alternate *I* contours.

1993ApJ...416..496C

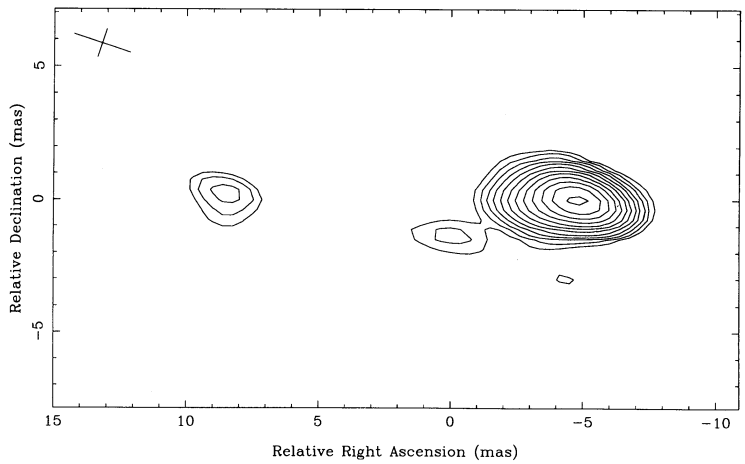

FIG. 3*a*

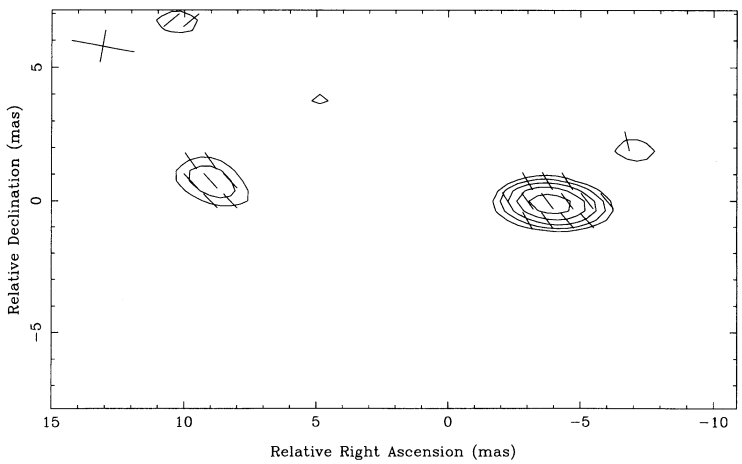

FIG. 3*b*

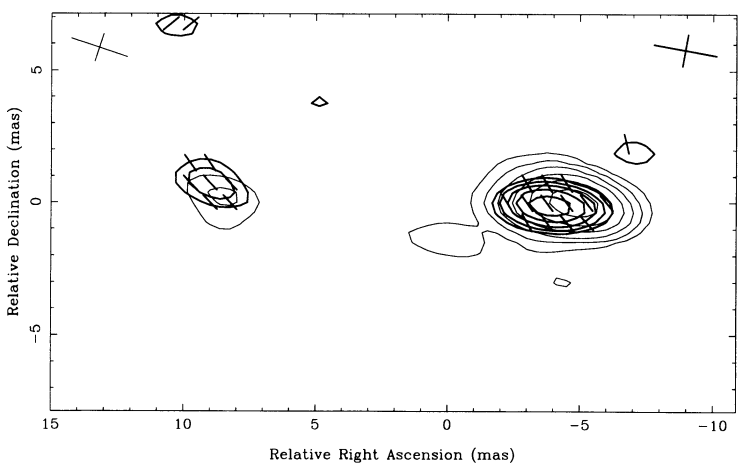

FIG. 3*c*

FIG. 3.—VLBI images of 0212+735 at 5 GHz, epoch 1984.23. (*a*) Total intensity, with contours at −2.0, 2.0, 2.8, 4.0, 5.7, 8.0, 11, 16, 22, 32, 45, 64, and 91% of the peak brightness of 1200 mJy beam^{-1}. (*b*) Linear polarization, with contours of polarized intensity at 20, 28, 40, 57, and 80% of the peak brightness of 24.4 mJy beam^{-1}, and sticks showing the orientations χ of the electric vectors (corrected for a rotation measure of +14 rad m^{-2}). (*c*) Superposition of the linear polarization image (*bold*) over the total intensity image, using only alternate *I* contours.

© American Astronomical Society • Provided by the NASA Astrophysics Data System

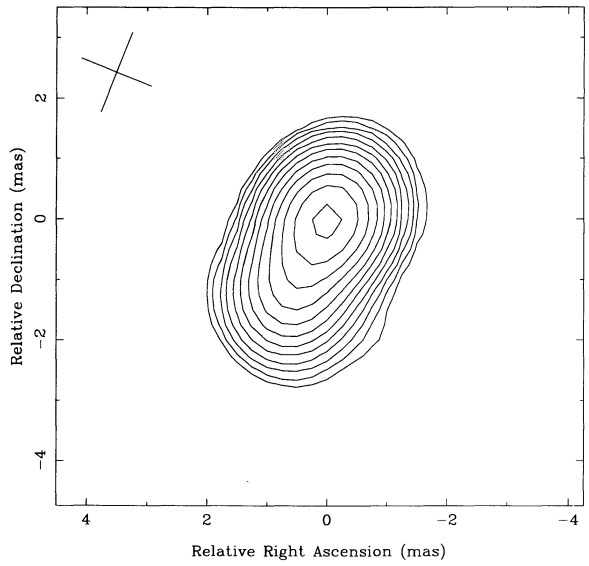

FIG. 4a

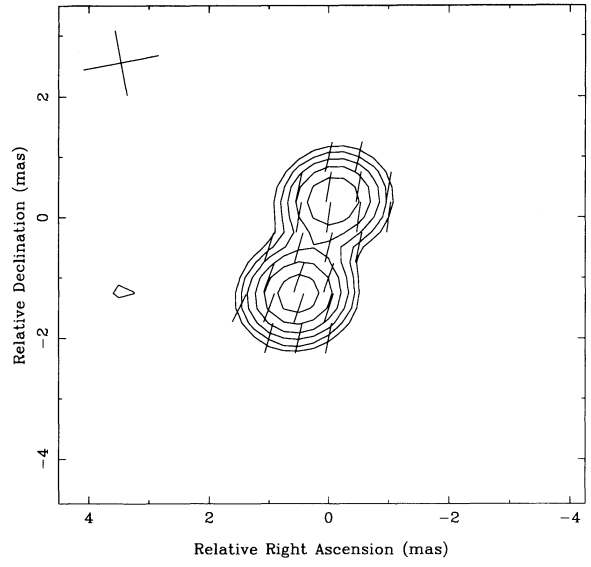

FIG. 4b

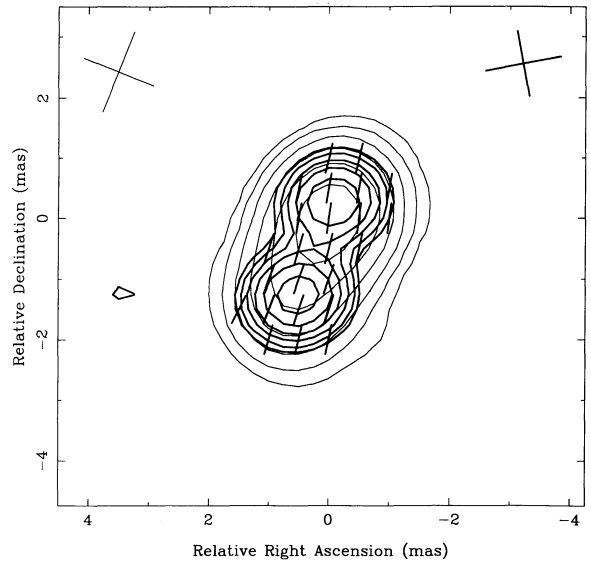

FIG. 4c

FIG. 4.—VLBI images of 0454+844 at 5 GHz, epoch 1984.78. (*a*) Total intensity, with contours at −2.0, 2.0, 2.8, 4.0, 5.7, 8.0, 11, 16, 22, 32, 45, 64, and 91% of the peak brightness of 391 mJy beam^{-1}. (*b*) Linear polarization, with contours of polarized intensity at 14, 20, 28, 40, 57, and 80% of the peak brightness of 10.5 mJy beam^{-1}, and sticks showing the orientations χ of the electric vectors (corrected for a rotation measure of +5 rad m^{-2}). (*c*) Superposition of the linear polarization image (*bold*) over the total intensity image, using only alternate *I* contours.

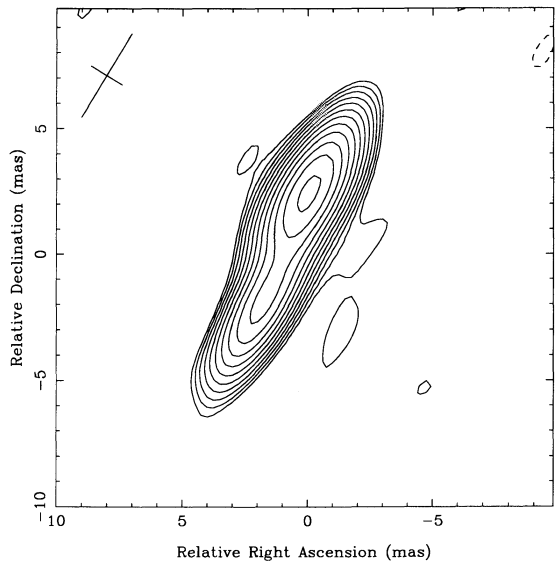

FIG. 5a

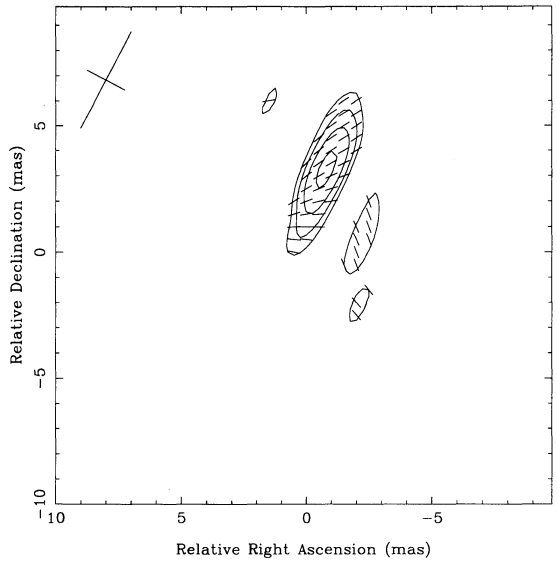

FIG. 5b

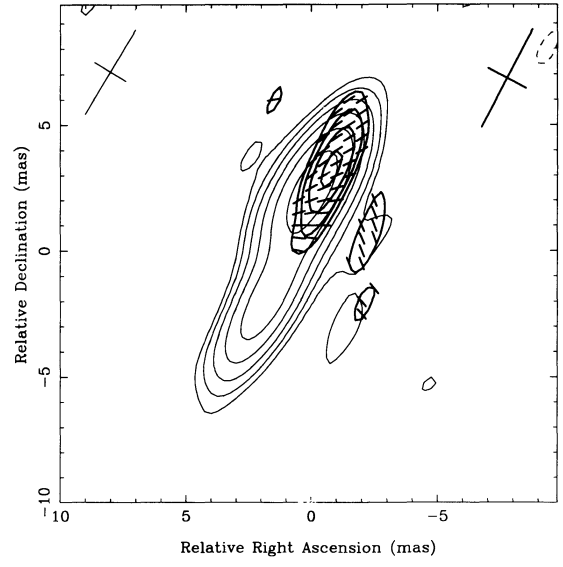

FIG. 5c

FIG. 5.—VLBI images of 0711+356 at 5 GHz, epoch 1984.23. (*a*) Total intensity, with contours at −2.0, 2.0, 2.8, 4.0, 5.7, 8.0, 11, 16, 22, 32, 45, 64, and 91% of the peak brightness of 438 mJy beam^{-1}. (*b*) Linear polarization, with contours of polarized intensity at 32, 45, 64, and 91% of the peak brightness of 12.5 mJy beam^{-1}, and sticks showing the orientations χ of the electric vectors (corrected for a rotation measure of +51 rad m^{-2}). (*c*) Superposition of the linear polarization image (*bold*) over the total intensity image, using only alternate *I* contours.

© American Astronomical Society • Provided by the NASA Astrophysics Data System

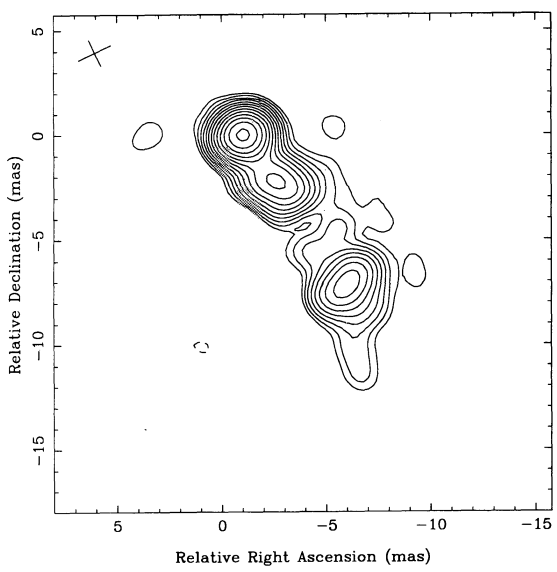

FIG. 6a

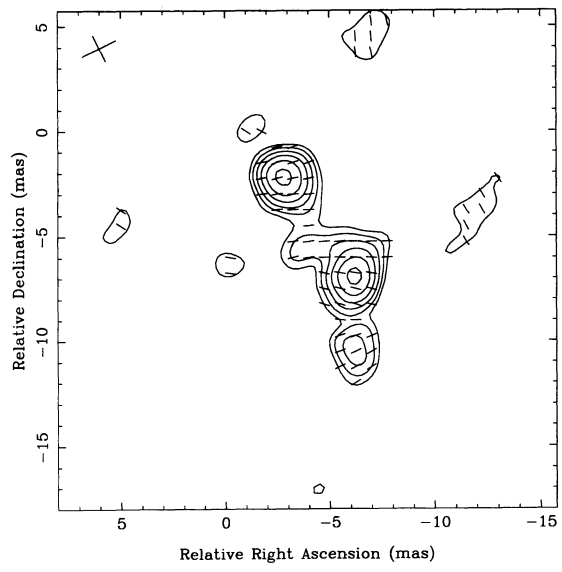

FIG. 6b

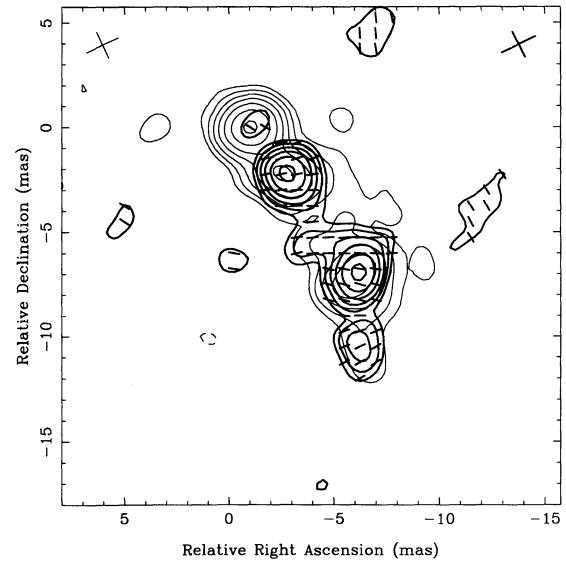

FIG. 6c

FIG. 6.—VLBI images of 0836+710 at 5 GHz, epoch 1984.23. (*a*) Total intensity, with contours at −1.4, 1.4, 2.0, 2.8, 4.0, 5.7, 8.0, 11, 16, 22, 32, 45, 64, and 91% of the peak brightness of 750 mJy beam^{-1}. (*b*) Linear polarization, with contours of polarized intensity at 16, 22, 32, 45, 64, and 91% of the peak brightness of 25.0 mJy beam^{-1}, and sticks showing the orientations χ of the electric vectors (corrected for a rotation measure of −9 rad m^{-2}). (*c*) Superposition of the linear polarization image (*bold*) over the total intensity image, using only alternate *I* contours.

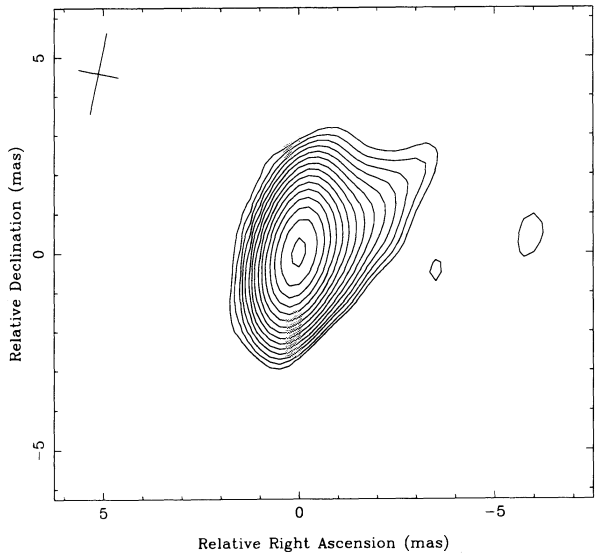

FIG. 7a

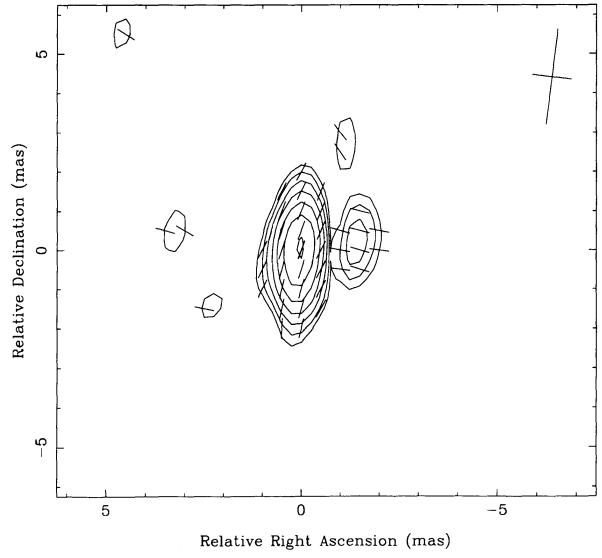

FIG. 7b

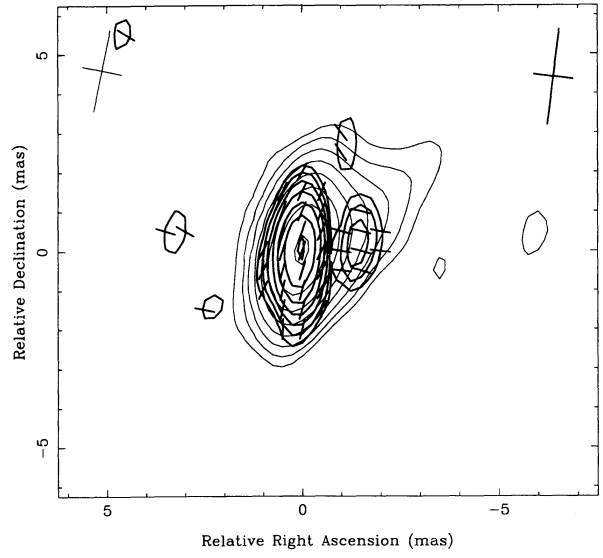

FIG. 7c

FIG. 7.—VLBI images of 0954+658 at 5 GHz, epoch 1987.41. (*a*) Total intensity, with contours at −0.7, 0.7, 1.0, 1.4, 2.0, 2.8, 4.0, 5.7, 8.0, 11, 16, 22, 32, 45, 64, and 91% of the peak brightness of 657 mJy beam^{-1}. (*b*) Linear polarization, with contours of polarized intensity at 12, 17, 24, 33, 48, 67, and 96% of the peak brightness of 45.1 mJy beam^{-1}, and sticks showing the orientations χ of the electric vectors (corrected for a rotation measure of −15 rad m^{-2}). (*c*) Superposition of the linear polarization image (*bold*) over the total intensity image, using only alternate *I* contours.

© American Astronomical Society • Provided by the NASA Astrophysics Data System

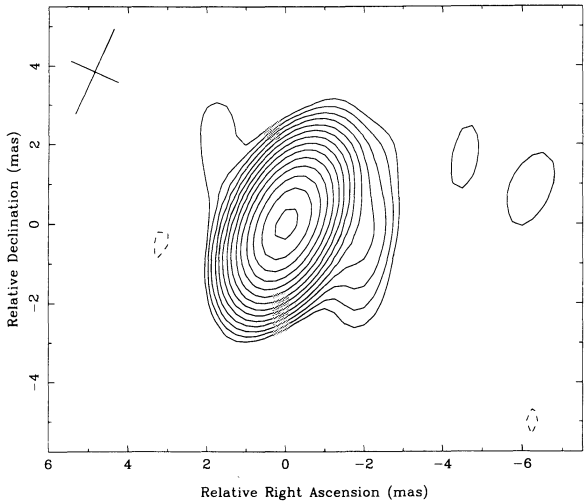

FIG. 8a

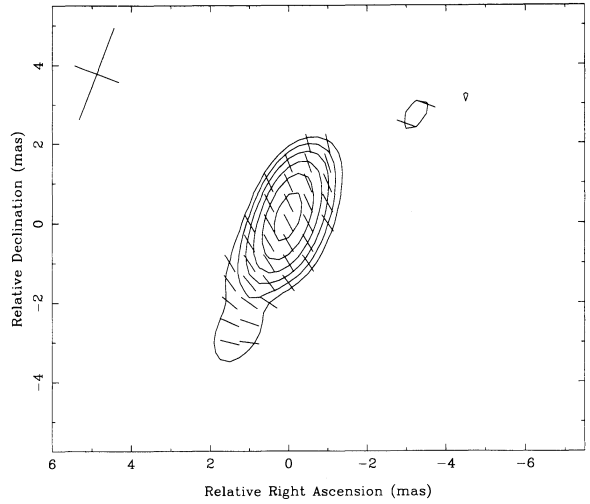

FIG. 8b

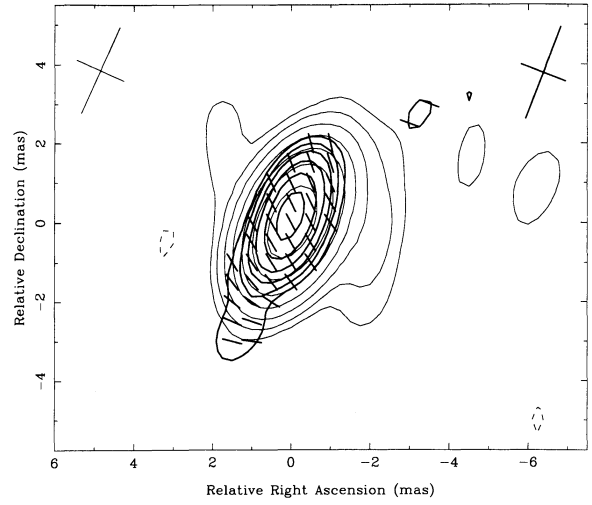

FIG. 8c

FIG. 8.—VLBI images of 1633+382 at 5 GHz, epoch 1984.78. (*a*) Total intensity, with contours at −1.0, 1.0, 1.4, 2.0, 2.8, 4.0, 5.7, 8.0, 11, 16, 22, 32, 45, 64, and 91% of the peak brightness of 2350 mJy beam^{-1}. (*b*) Linear polarization, with contours of polarized intensity at 15, 21, 30, 42, 60, and 85% of the peak brightness of 33.8 mJy beam^{-1}, and sticks showing the orientations χ of the electric vectors (corrected for a rotation measure of +4 rad m^{-2}). (*c*) Superposition of the linear polarization image (*bold*) over the total intensity image, using only alternate *I* contours.

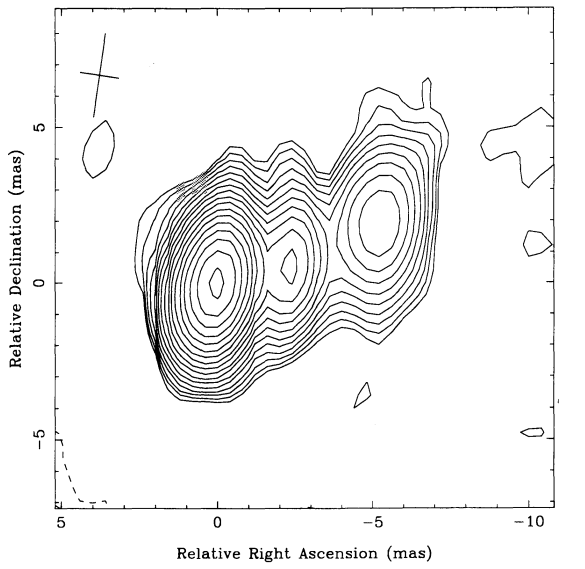

FIG. 9a

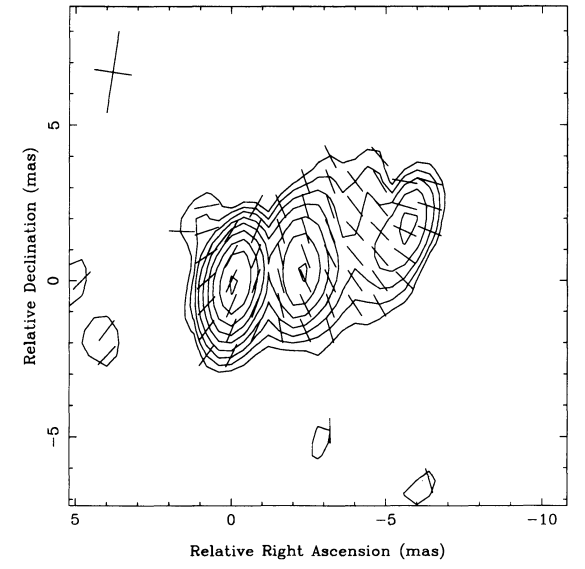

FIG. 9b

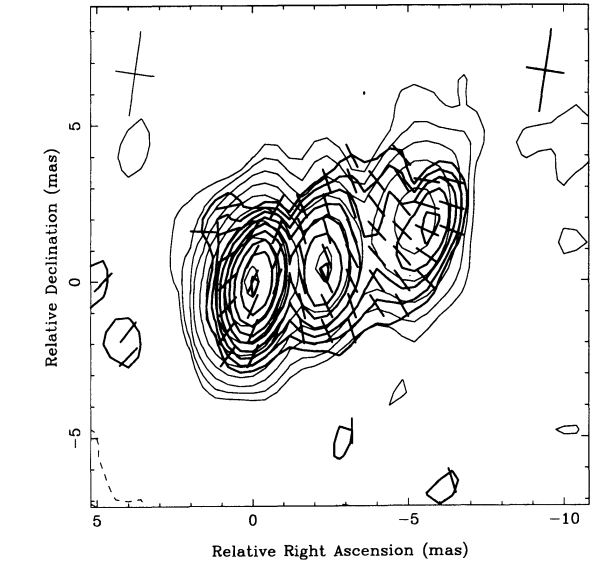

FIG. 9c

FIG. 9.—VLBI images of 1641+399 at 5 GHz, epoch 1984.23. (*a*) Total intensity, with contours at −0.35, 0.35, 0.5, 0.7, 1.0, 1.4, 2.0, 2.8, 4.0, 5.7, 8.0, 11, 16, 22, 32, 45, 64, and 91% of the peak brightness of 6940 mJy beam^{-1}. (*b*) Linear polarization, with contours of polarized intensity at 6.0, 8.5, 12, 17, 24, 34, 48, 68, and 96% of the peak brightness of 167 mJy beam^{-1}, and sticks showing the orientations χ of the electric vectors (corrected for a rotation measure of +26 rad m^{-2}). (*c*) Superposition of the linear polarization image (*bold*) over the total intensity image, using only alternate *I* contours.

© American Astronomical Society • Provided by the NASA Astrophysics Data System

© American Astronomical Society • Provided by the NASA Astrophysics Data System

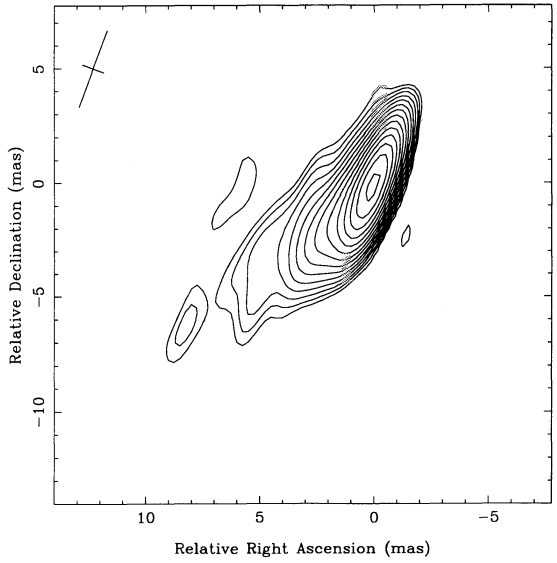

FIG. 10

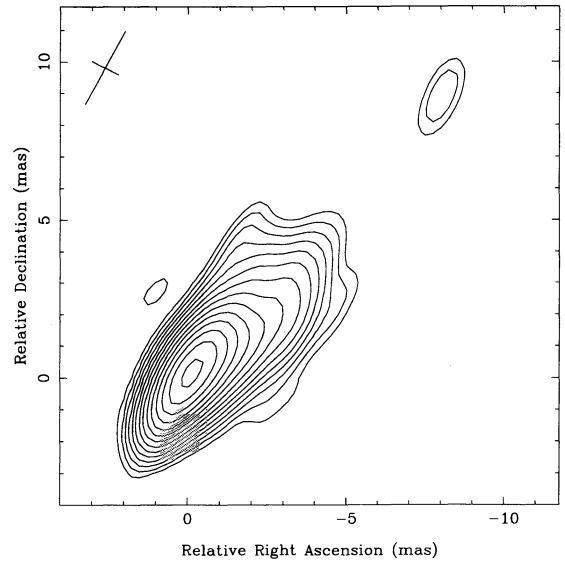

FIG. 11

FIG. 10.—VLBI image of 1652+398 at 5 GHz, epoch 1987.41. Total intensity, with contours at −1.0, 1.0, 1.4, 2.0, 2.8, 4.0, 5.7, 8.0, 11, 16, 22, 32, 45, 64, and 91% of the peak brightness of 537 mJy beam^{-1}.
FIG. 11.—VLBI image of 1749+701 at 5 GHz, epoch 1987.41. Total intensity, with contours at −1.0, 1.0, 1.4, 2.0, 2.8, 4.0, 5.7, 8.0, 11, 16, 22, 32, 45, 64, and 91% of the peak brightness of 279 mJy beam^{-1}.

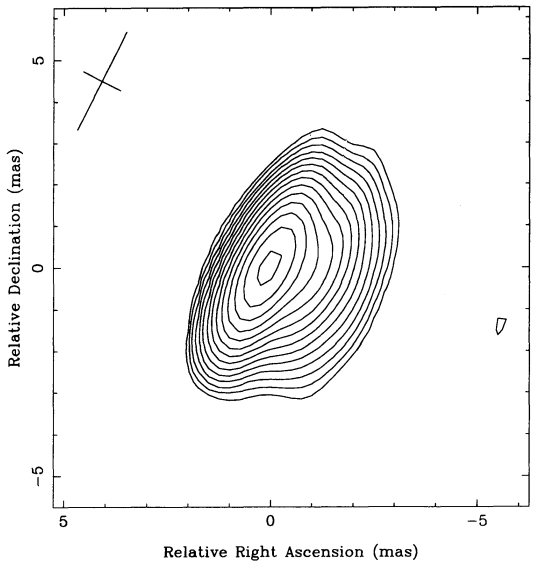

FIG. 12*a*

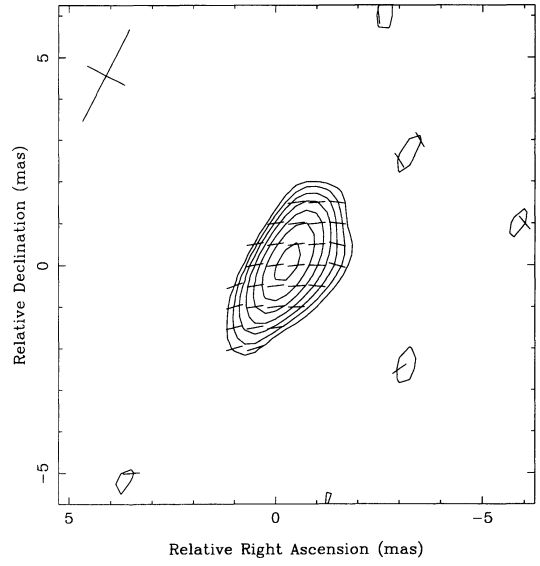

FIG. 12*b*

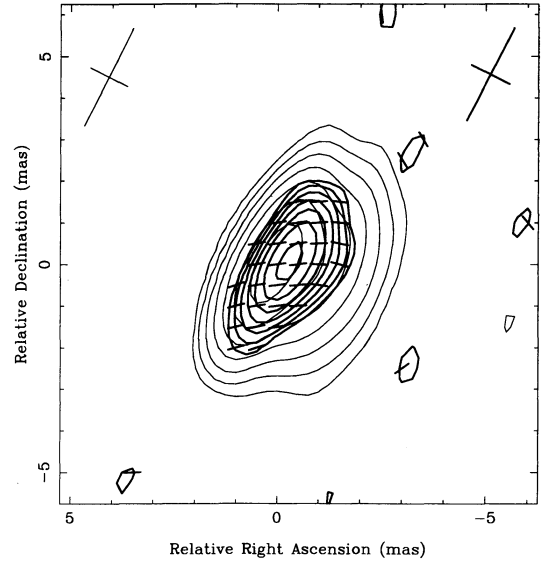

FIG. 12*c*

FIG. 12.—VLBI images of 1803+784 at 5 GHz, epoch 1987.41. (*a*) Total intensity, with contours at −1.0, 1.0, 1.4, 2.0, 2.8, 4.0, 5.7, 8.0, 11, 16, 22, 32, 45, 64, and 91% of the peak brightness of 1440 mJy beam^{-1}. (*b*) Linear polarization, with contours of polarized intensity at 11, 16, 22, 31, 44, 62, and 89% of the peak brightness of 61.4 mJy beam^{-1}, and sticks showing the orientations χ of the electric vectors (corrected for a rotation measure of −70 rad m^{-2}). (*c*) Superposition of the linear polarization image (*bold*) over the total intensity image, using only alternate *I* contours.

1993ApJ...416..496C

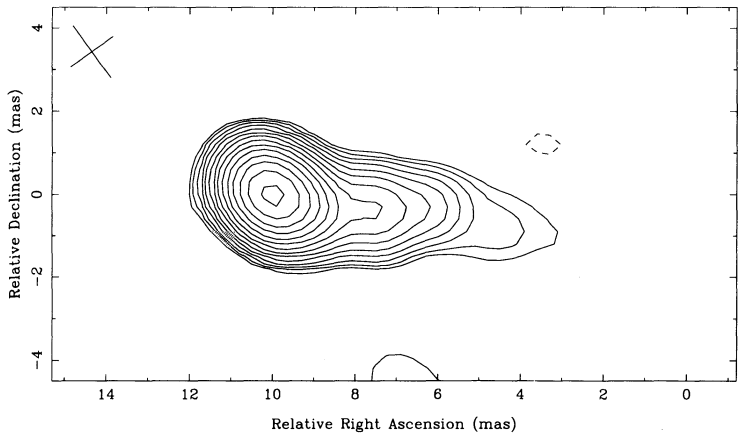

FIG. 13*a*

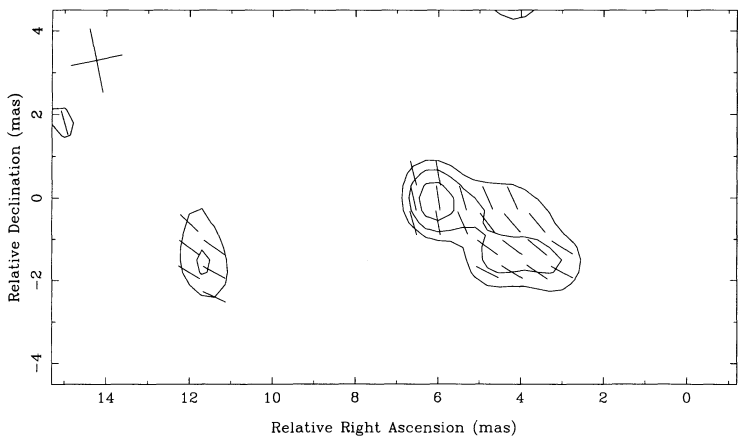

FIG. 13*b*

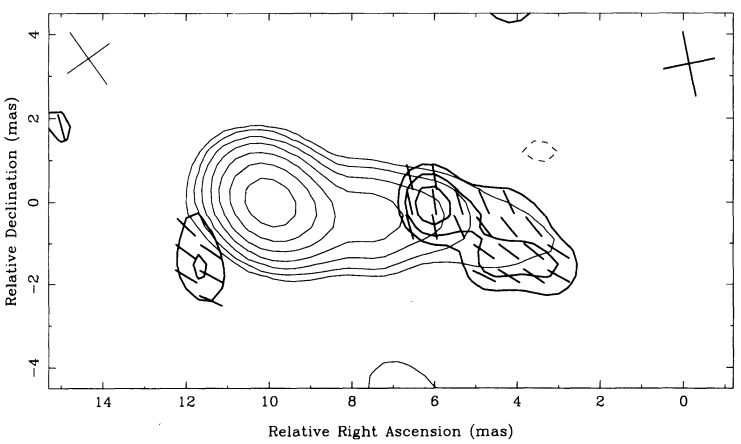

FIG. 13*c*

FIG. 13.—VLBI images of 1807+698 at 5 GHz, epoch 1984.23. (*a*) Total intensity, with contours at −1.0, 1.0, 1.4, 2.0, 2.8, 4.0, 5.7, 8.0, 11, 16, 22, 32, 45, 64, and 91% of the peak brightness of 750 mJy beam^{-1}. (*b*) Linear polarization, with contours of polarized intensity at 40, 57, and 80% of the peak brightness of 6.5 mJy beam^{-1}, and sticks showing the orientations χ of the electric vectors (uncorrected for rotation measure). (*c*) Superposition of the linear polarization image (*bold*) over the total intensity image, using only alternate *I* contours.

© American Astronomical Society • Provided by the NASA Astrophysics Data System

© American Astronomical Society • Provided by the NASA Astrophysics Data System

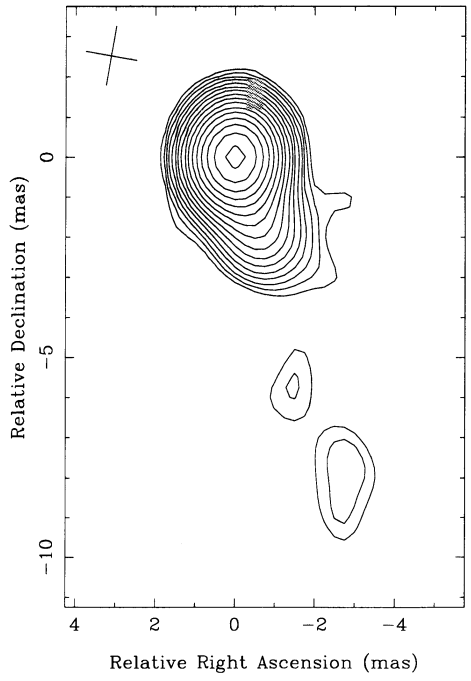

FIG. 14*a*

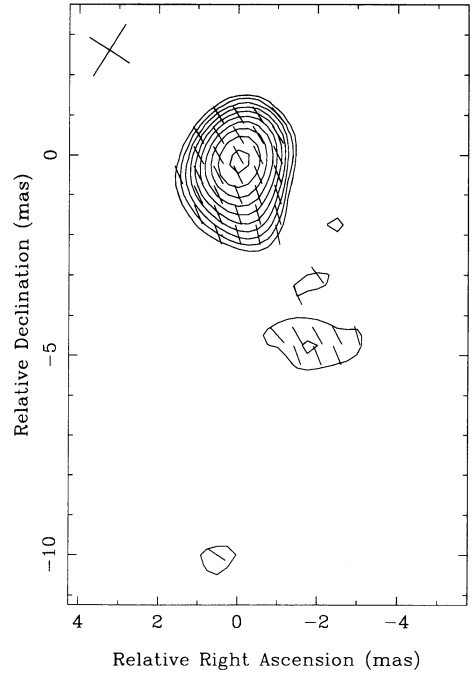

FIG. 14*b*

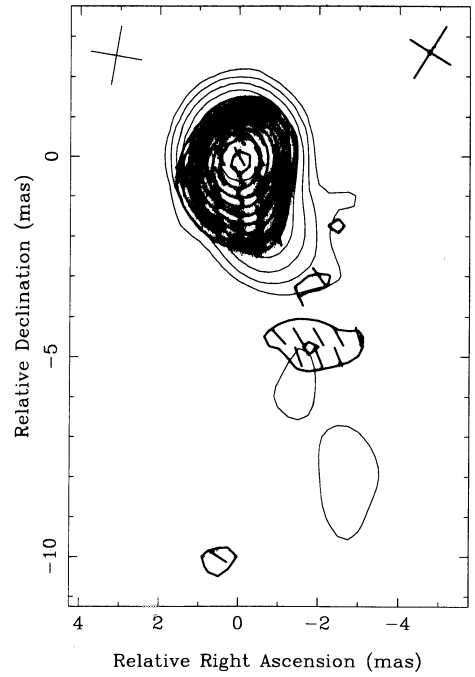

FIG. 14*c*

FIG. 14.—VLBI images of 1823 + 568 at 5 GHz, epoch 1984.78. (*a*) Total intensity, with contours at −0.5, 0.5, 0.7, 1.0, 1.4, 2.0, 2.8, 4.0, 5.7, 8.0, 11, 16, 22, 32, 45, 64, and 91% of the peak brightness of 789 mJy beam^{-1}. (*b*) Linear polarization, with contours of polarized intensity at 4.0, 5.7, 8.0, 11, 16, 22, 32, 45, 64, and 91% of the peak brightness of 41.8 mJy beam^{-1}, and sticks showing the orientations χ of the electric vectors (corrected for a rotation measure of +33 rad m^{-2}). (*c*) Superposition of the linear polarization image (*bold*) over the total intensity image, using only alternate *I* contours.

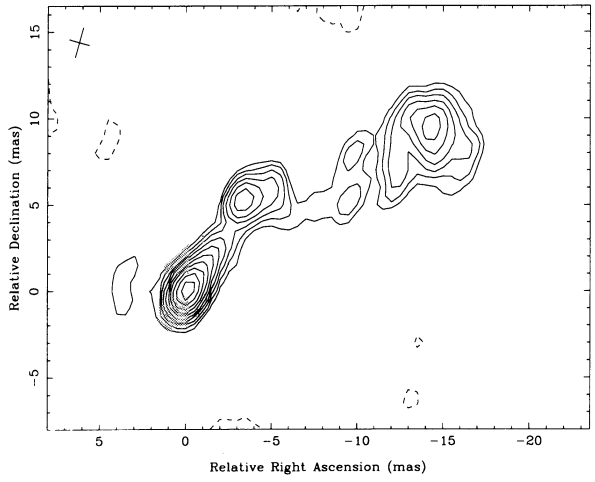

FIG. 15*a*

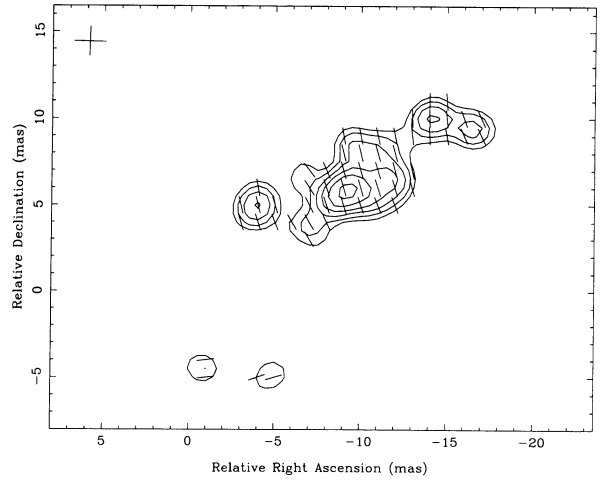

FIG. 15*b*

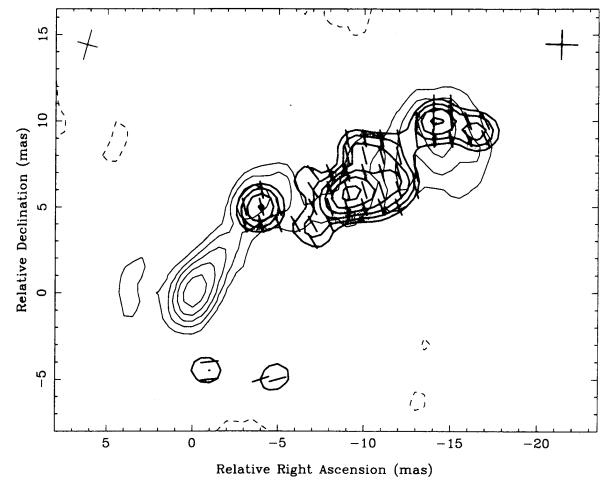

FIG. 15*c*

FIG. 15.—VLBI images of 1828 + 487 at 5 GHz, epoch 1984.78. (*a*) Total intensity, with contours at −3.5, 3.5, 5.0, 7.0, 9.9, 14, 20, 28, 40, 56, and 79% of the peak brightness of 529 mJy beam^{-1}. (*b*) Linear polarization, with contours of polarized intensity at 16, 22, 32, 45, 64, and 91% of the peak brightness of 17.6 mJy beam^{-1}, and sticks showing the orientations χ of the electric vectors (corrected for a rotation measure of +130 rad m^{-2}). (*c*) Superposition of the linear polarization image (*bold*) over the total intensity image, using only alternate *I* contours.

© American Astronomical Society • Provided by the NASA Astrophysics Data System

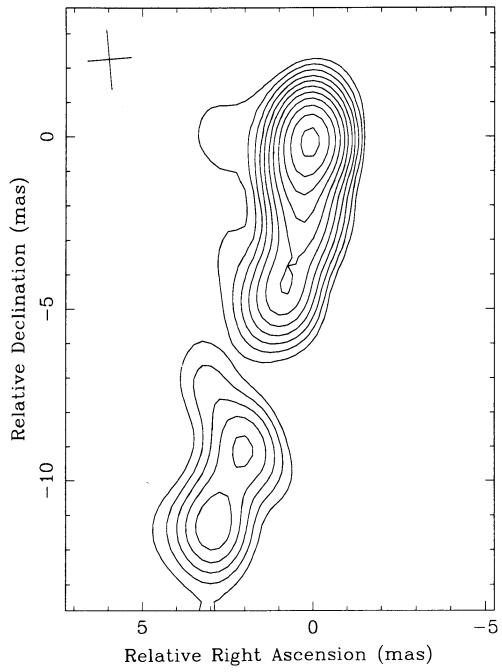

FIG. 16*a*

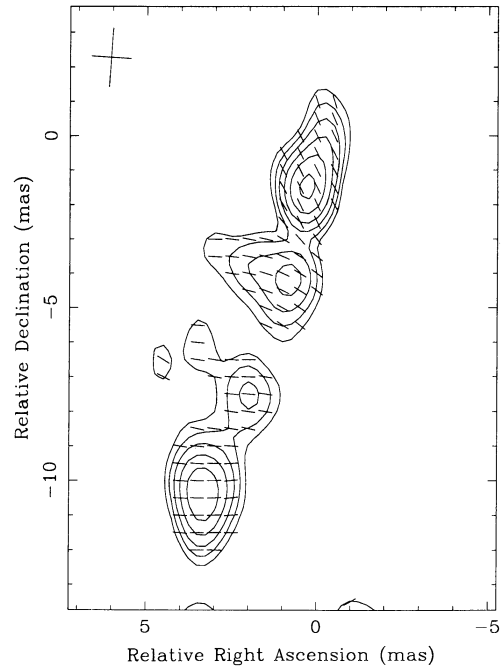

FIG. 16*b*

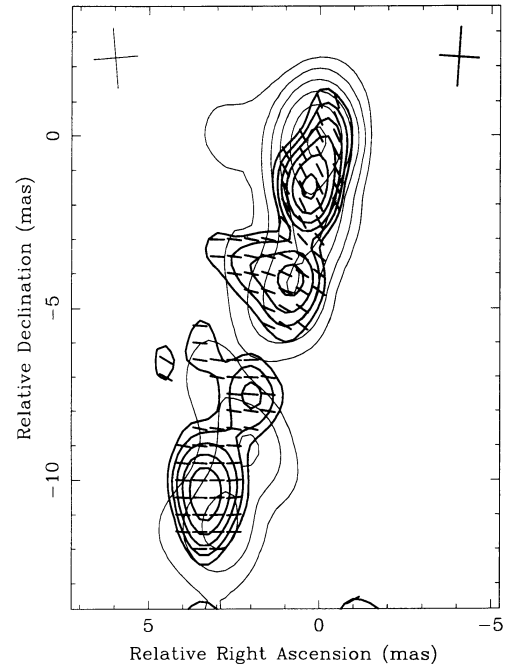

FIG. 16*c*

FIG. 16.—VLBI images of 1928+738 at 5 GHz, epoch 1984.23. (*a*) Total intensity, with contours at −2.8, 2.8, 4.0, 5.7, 8.0, 11, 16, 22, 32, 45, 64, and 91% of the peak brightness of 958 mJy beam^{-1}. (*b*) Linear polarization, with contours of polarized intensity at 16, 22, 32, 45, 64, and 91% of the peak brightness of 26.2 mJy beam^{-1}, and sticks showing the orientations χ of the electric vectors (corrected for a rotation measure of +31 rad m^{-2}). (*c*) Superposition of the linear polarization image (*bold*) over the total intensity image, using only alternate *I* contours.

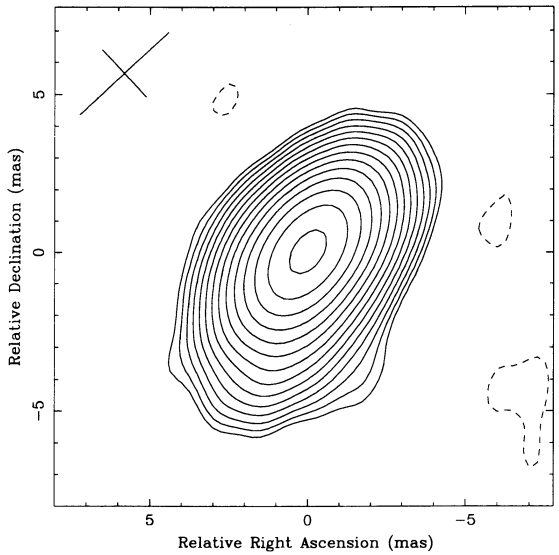

FIG. 17*a*

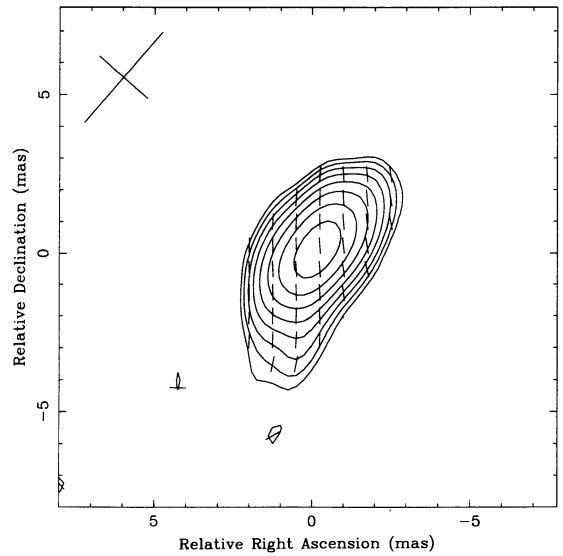

FIG. 17*b*

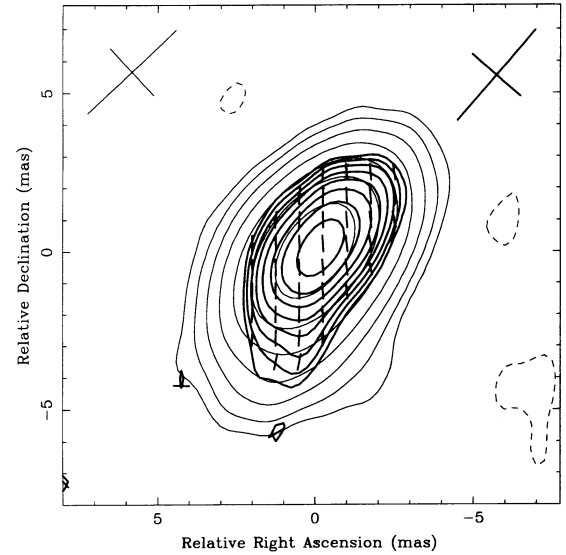

FIG. 17*c*

FIG. 17.—VLBI images of 2200+420 at 5 GHz, epoch 1984.23. (*a*) Total intensity, with contours at −1.0, 1.0, 1.4, 2.0, 2.8, 4.0, 5.7, 8.0, 11, 16, 22, 32, 45, 64, and 91% of the peak brightness of 1720 mJy beam^{-1}. (*b*) Linear polarization, with contours of polarized intensity at 7.1, 10, 14, 20, 28, 40, 57, and 80% of the peak brightness of 93.0 mJy beam^{-1}, and sticks showing the orientations χ of the electric vectors (corrected for a rotation measure of −205 rad m^{-2}). (*c*) Superposition of the linear polarization image (*bold*) over the total intensity image, using only alternate *I* contours.

1993ApJ...416..496C

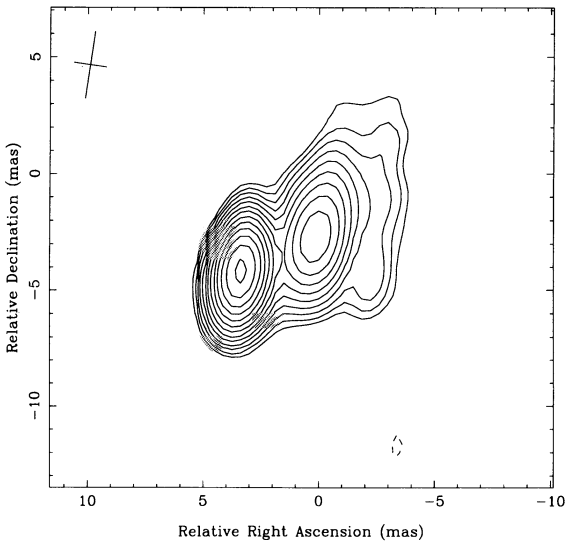

FIG. 18*a*

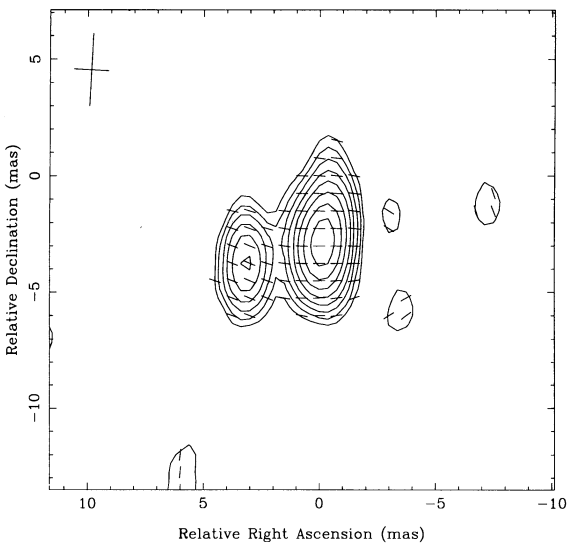

FIG. 18*b*

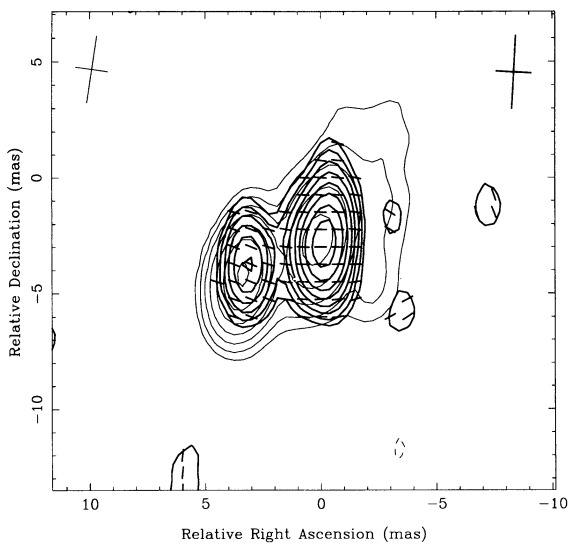

FIG. 18*c*

FIG. 18.—VLBI images of 2351+456 at 5 GHz, epoch 1984.78. (*a*) Total intensity, with contours at −1.4, 1.4, 2.0, 2.8, 4.0, 5.7, 8.0, 11, 16, 22, 32, 45, 64, and 91% of the peak brightness of 547 mJy beam^{-1}. (*b*) Linear polarization, with contours of polarized intensity at 7.1, 10, 14, 20, 28, 40, 57, and 80% of the peak brightness of 16.1 mJy beam^{-1}, and sticks showing the orientations χ of the electric vectors (uncorrected for a rotation measure). (*c*) Superposition of the linear polarization image (*bold*) over the total intensity image, using only alternate *I* contours.

small. See also the discussion of § 3 of Paper II). We have made no correction for the Ricean noise bias in p (see Wardle & Kronberg 1974). No value of m smaller than 0.5% should be trusted, owing to residual errors in the polarization calibration. For weaker or extended features, the errors may be larger.

The term "position angle" can refer, of course, to either a structural position angle or a polarization position angle (electric vectors). To avoid confusion, we denote structural position angles by θ and polarization position angles by χ. References to optical data can be found in PR88. For linear dimensions we assume $H_0 = 100\ h$ km s^{-1} Mpc^{-1} and $q_0 = 0.5$. The spectral index, α, is defined as $S \propto \nu^{+\alpha}$.

0016+731.—This source is a high-redshift 18 mag quasar ($z = 1.781$; 1 mas = 4.2 h^{-1} pc). It shows significant intraday variability (Witzel 1990). PR88 place it in their "very compact" category, defined as having more than 90% of its flux in the core ($F_c > 0.9$). *I* and *P* images are shown in Figures 1*a*–1*c*. The *I* image shows a bright component in the north, a clear extension almost due south, and also signs of extension southeast of the northernmost component. A three-component model provides a very good fit to the data (Table 4). The flux density of the core has declined by about 0.5 Jy since the observations by PR88 (epoch 1980.74), and they would now classify it on the boundary between "compact" ($0.8 < F_c < 0.9$) and "asymmetric I" ($0.5 < F_c < 0.8$). The southeast component (SE) is almost certainly real, since PR88 found the core to be slightly extended at this position angle. Indeed, it is possible that the "jet" trajectory is strongly curved on milliarcsecond scales, emerging at position angle $\theta \simeq 100°$ and bending through $\sim 90°$ toward the southwest. Taking at face value the locations of the southern component (S) given in Table 4 and by PR88, its proper motion is $\mu \simeq 0.22$ mas yr^{-1} in a nonradial trajectory, corresponding to superluminal motion with $\beta_{\rm app} \simeq 8\ h^{-1}$. Of course further observations are essential to confirm this and the true direction of the jet. No extended structure has been detected on arcsecond scales (Perley 1982).

The *P* image shows a single, weak component displaced from the peak in *I* by 0.3 mas (about one-fifth of a beam) to the northeast. If we identify the peaks in *I* and *P* with the same component, it is 1.7% polarized. No significant polarization is detected from the S component ($m < 4\%$).

0108+388 = OC 314.—This source is identified with a 22 mag galaxy with $z = 0.669$ (C. R. Lawrence 1992, private communication). PR88 found two components separated by 5 mas, with steep high-frequency spectra, which contained essentially all the single-dish flux (category "compact S double"). At frequencies below 1 GHz, the VLBI source has the most steeply rising spectrum ($\alpha \simeq 2.1$) yet observed in an AGN (Baum et al. 1990). The rather sparse data in our observations (from 1984 October) do not constrain the source structure well,

© American Astronomical Society • Provided by the NASA Astrophysics Data System

1993ApJ...416..496C

but they are consistent with the image presented by PR88. We show no images of this source here. VLA measurements find that the source is very weakly polarized (less than 0.2%; Perley 1982), and measurements at the VLA during our observations are consistent with this result. The polarized visibilities constrain any polarized feature on VLBI scales to be weaker than 4 mJy. Perley (1982) detected no extended structure using the VLA, although deeper observations by Baum et al. (1990) found diffuse emission 20″ east of the core.

0133+476 = DA 55 = OC 457.—This 18 mag object is a quasar with a redshift of $z = 0.859$ (1 mas = 4.2 h^{-1} pc) (Lawrence et al. 1986) and was found by Impey & Tapia (1990) to have an unusually high optical polarization ($m_{opt} = 20.8\%$ at position angle $\chi = 67°$). *I* and *P* images are shown in Figures 2*a*–2*c*. In total intensity the source is clearly double with separation 1.3 mas at position angle $\theta \simeq -55°$. PR88 classify this source as "compact." They found a strong core, elongated at position angle $\theta = -32°$, a weak component 3.7 mas distant at position angle $\theta = -43°$, and evidence of additional diffuse structure farther to the west. Since their observations (epoch 1978.95), their second component appears to have faded and the core has declined by 600 mJy. It would now be classified as "asymmetric I." Perley (1982) detected no extended emission on arcsecond scales.

A polarized flux of 14 mJy is detected in the brighter component, making it 1.8% polarized. The *P* image has been corrected for 23° of Faraday rotation (rotation measure [RM] = 109 ± 3 rad m^{-2}; Rusk 1988). The resulting position angle of polarization is $\chi = 112°$, which makes an angle of 10° with the jet direction. Since this component is presumably the core, the polarization may represent an emerging component that is still opaque.

The total fluxes seen at the VLA were $I = 1.34$ Jy and $P = 24$ mJy at position angle $\chi = 130°$. Subtracting from these the sums of the clean components in the *I* and *P* images, we find that the intermediate-scale structure (from 10 to ~1000 mas) contains about 330 mJy in total intensity and 21 mJy in polarized intensity ($m \simeq 6\%$) at position angle $\chi = 113°$ (see Table 5). Applying Rusk's value for the rotation measure, the intrinsic position angle is $\chi = 66°$, which is oriented at ~60° to the direction of the jet on milliarcsecond scales.

0153+744.—This is a high-redshift 16 mag quasar ($z = 2.338$, 1 mas = 3.9 h^{-1} pc). The *I* image is similar to those of Hummel et al. (1988), and shows a bright core component and a jet that curves from an initial easterly to a southwesterly direction, terminating in a bright but extended component. From less extensive observations, PR88 classify this source as a "compact F (flat spectrum) double," but it is clear from Hummel et al. that the flat-spectrum core and continuous jet place it in the "asymmetric II" category.

No polarized flux brighter than 3 mJy beam^{-1} was found on the *P* image, nor was any significant polarized flux detected at the VLA during the observations ($m < 0.4\%$). Since our observations have greatly inferior *u-v* coverage compared with those of Hummel et al., and no polarization was detected, neither the *I* nor the *P* image is shown here. Perley (1982) found no evidence for extended structure on arcsecond scales and found the source to be unpolarized at 5 and 1.4 GHz.

0212+735.—This is a high-redshift 19 mag quasar ($z = 2.367$; 1 mas = 3.9 h^{-1} pc) with particularly strong emission lines (Lawrence 1990). *I* and *P* images are shown in Figures 3*a*–3*c*. The *I* image agrees well with those by PR88 and Witzel et al. (1988). The main features are a bright core component in the west, a jet or string of components extending some 4 mas somewhat south of east from the core, and a weak component 15 mas to the west. Quite a good fit to the data was obtained with the five-component model shown in Table 4. The weak component K2 was unconstrained by the model-fitting program, and its flux and polarization were obtained by summing clean components.

From three observations at 5 GHz at epochs between 1979.93 and 1985.39, Witzel et al. (1988) find that the inner jet component increased its separation from the core from 1.0 to 1.5 mas, and deduce a proper motion of $\mu = 0.09 \pm 0.05$ mas yr^{-1} ($\beta_{app} \simeq 4\ h^{-1}$). This component is consistent with the *centroid* of our components K3 and K4. It is therefore possible that K3 and K4 represent a single extended component. In this case, our model fitting indicates that this component is more strongly polarized at its inner edge.

The outermost component (some 13 mas from the core) is also close to the position found by Witzel et al. (1988) and is coincident with a revised position from the PR88 observations, which were made in 1980.72 (T. J. Pearson 1992, private communication). This component appears to be stationary. It is clearly resolved in all observations, so it is difficult to assign a meaningful limit on the apparent velocity. On our images the *I* and *P* peaks are significantly displaced, suggesting that the polarization of the outer edge is much higher than the component's mean of 19%.

In the inner jet (K4), the projected magnetic field is offset from the jet direction by ~30°. For the outer component, K1, we do not know the local jet direction. If, as suggested by drawing a smooth line through the components, the jet is turning toward the northeast, then the projected magnetic field may be roughly parallel to the jet. The polarization of the intermediate-scale structure is significant ($p \simeq 20$ mJy at $\chi \simeq 42°$) but weak ($m \simeq 3\%$), and has nearly the same polarization position angle as K1. No arcsecond-scale structure was detected by either Perley (1982) or Antonucci et al. (1986).

0316+413 = 3C 84 = NGC 1275.—This nearby 11.9 mag galaxy ($z = 0.0172$) exhibits complex radio structure from submilliarcsecond scales to about 8′, oriented in a roughly north-south direction (e.g., Readhead et al. 1990; Krichbaum 1990). Proper motions have been detected corresponding to $\beta_{app} \simeq 0.5\ h^{-1}$ (Marr, Backer, & Wright 1990). 3C 84 is unpolarized at all radio wavelengths ($m < 0.2\%$; Altschuler & Wardle 1976; Aller et al. 1985), and we use it regularly as a calibrator for the instrumental polarization. It is heavily resolved on all baselines, and with our limited *u-v* coverage we make no attempt to construct an image.

0454+844.—This is a 16.5 mag BL Lacertae object with no measured redshift. No arcsecond-scale structure was detected by either Perley (1982) or Antonucci et al. (1986). Our observations of this source were discussed by GCRW89, and the images are reproduced here in Figures 4*a*–4*c*.

The radio source is highly variable on a time scale of months at centimeter wavelengths (Seielstad, Pearson, & Readhead 1983). The northwest component declined from 800 mJy (epoch 1979.93; Eckart et al. 1987) to 507 mJy (epoch 1981.64; PR 88), to 377 mJy (epoch 1984.77; this paper). The southeast component appears equally variable: 240 mJy, 523 mJy, and 137 mJy, respectively, at these epochs. It is unclear from these data which component is more likely to be the core. Eckart et al. (1987) also show an image at 22 GHz and compute apparent spectral indices of −0.7 for the northwest component and −0.2 for the southeast component, suggesting that the latter

© American Astronomical Society • Provided by the NASA Astrophysics Data System

1993ApJ...416..496C

should be identified with the core. However, in view of the rapid variability of this source and the long interval (3 years) between the observations, this inference may not be correct. Our polarization data suggest that the stronger northwest component is in fact the core. Then the fractional polarizations of the "core" and "jet" (2.3% and 8.5%, respectively) are in line with other BL Lacertae objects we have imaged (GCRW89; Roberts et al. 1990b; GCRW92). The polarization position angles of both components lie within 10° of the structural axis.

Combining the observations shown here with those made in *I* by other observers (PR88; Eckart et al. 1986, 1987) yields an apparent separation speed of $\mu = 0.14 \pm 0.04$ mas yr^{-1} (GCRW89). This source is superluminal if its redshift is greater than $z = 0.17$ (Witzel et al. 1988).

0711+356 = OI 318.—This is a 17 mag quasar with a redshift of $z = 1.62$ (1 mas = 4.2 h^{-1} pc). *I* and *P* images are shown in Figures 5*a*–5*c*. The source has a double structure, and polarization is detected from the brighter (northern) component. Comparison of 10.7 and 5 GHz images shows that the southern component has the flatter spectrum, suggesting that it is the core (PR88); this result is consistent with the detection of polarized flux ($m = 2.5\%$) in only the northern component (although we note that the upper limit on the degree of polarization from the weak southern component is in fact 2.6%). The polarization position angle in the jet ($\chi = 116°$) bears no obvious relation to the structural position angle ($\theta = -22°$).

Model fits in the *u-v* plane to this source were attempted but were not very successful. The reason seems to be that the clean components are distributed quasi-continuously along the jet (PR88 fitted four components to this source). The component fluxes listed in Table 4 were estimated by summing the clean components. The listed separation is that of the peaks in the distribution of clean components. It is interesting that this continues the trend noted by PR88 that this source gives the appearance of superluminal contraction. They found separations from the core of 5.35 mas (epoch 1980.53) and 5.17 mas (epoch 1982.95; see also Readhead, Pearson, & Unwin 1984) for the strongest component; we find 4.8 mas (epoch 1984.23). This corresponds to $\beta_{app} \simeq -5\,h^{-1}$, although it is possible that this effect is simply due to changes in the brightness distribution of the complex jet. Further observations are clearly warranted.

0836+710 = 4C 71.07.—This is a 16.5 mag quasar with a redshift of $z = 2.17$ (1 mas = 4.0 h^{-1} pc). It is strongly polarized at all radio wavelengths (e.g., Rusk 1988) but not at optical wavelengths (based on a single measurement by Impey & Tapia 1990). Our observations reveal a rich structure with several strongly polarized components, shown in Figures 6*a*–6*c*. In total intensity, our image agrees well with those by Krichbaum et al. (1990). The source shows a bright core slightly extended to the south (K4); two bright knots, K3 and K2; and a fainter extension farther to the south, which we call K1.

The fractional polarization rises with increasing distance from the core, which is less than 1% polarized. The innermost knot, K4, is less than 3.3% polarized. K3 is about 12% polarized ($\chi = 96°$), and K2 is about 13% polarized. There is a gradient in electric vector orientation from $\chi = 90°$ to $\chi = 70°$ across K2. At K1 $m \simeq 69\%$, indicating an almost perfectly ordered magnetic field. The high degree of polarization of K1 is confirmed by new observations (Cawthorne 1993). The inferred magnetic field orientation appears to be offset from the direction of the jet by about 40° in the region of K2 and K3.

The peaks of emission of the core, K2 and K3 lie nearly on a straight line along position angle $\theta \simeq -145°$, and the peaks of polarized and total intensity are coincident to within a small fraction of a beamwidth. However, the more diffuse emission around these shows some tendency to oscillate from side to side, moving to the southeast between the core and K3 and to the northwest between K3 and K2. At K1 the bending is quite clear. The 5 GHz observations by Krichbaum et al. (1990) also show this structure, with the jet bending back to position angle $\theta \simeq 200°$ after K1. It is therefore conceivable that in K2 and K1 the normals to the observed electric vectors do in fact trace out a longitudinal magnetic field in a wiggling jet. However, in K3 the magnetic field does appear to be oblique to the local jet direction, unless the negligible correction we have used for Faraday rotation is inappropriate.

The positions of components K2 and K3 are consistent with the results of Krichbaum et al. (1990). They show (from images at several epochs) that while K3 (their component C) appears to be stationary, K2 (their component D) is moving radially outward at $\mu = 0.14 \pm 0.05$ mas yr^{-1}, which corresponds to an apparent speed $\beta_{app} = 5.9\,h^{-1}$. These authors also noted the appearance of a new component (which they call component B), 0.8 mas from the core in their epoch 1985.4 image, for which they deduce an apparent velocity $\beta_{app} = 9.5\,h^{-1}$. In our image this component is also present as the core's extension in the direction of the jet. In the distribution of clean components, K4 appears as a detached clump with $I \simeq 150$ mJy, located 0.8 ± 0.3 mas from the core. No significant polarized emission is detected from this component ($m < 3.3\%$).

Krichbaum et al. (1990) also show images made at 1.6 and 0.3 GHz. At 0.3 GHz, they follow the jet out to at least 180 mas. On these scales the direction of the jet is more nearly south ($\theta \simeq 195°$–$200°$). We note that the magnetic field direction inferred from our image lies within a few degrees of the direction of the jet on much larger scales; the jet gives the appearance of anticipating the direction it will follow a long way downstream. Arcsecond-scale observations with MERLIN (Krichbaum et al. 1990) and the VLA (Perley 1982; Rusk 1988; O'Dea, Barvainis, & Challis 1988) show a single detached component 1".5 from the core at position angle 200°. Hummel et al. (1992) show new images of 0836+710 made from a combination of VLBI and MERLIN data at 5 GHz. These show the gentle curving of the jet as well as two kinks which may result from magnetohydrodynamic instabilities, perhaps stabilized by longitudinal magnetic fields.

The total fluxes in *I* and *P* recorded by the VLA during our observations and those derived from the VLBI images are shown in Table 5. Some 34% of the *I* flux and 50% of the total *P* flux seen by the VLA are not found in the VLBI images. Thus, on intermediate scales, the jet contains 88 mJy of polarized flux ($m \simeq 12\%$) at position angle $\chi = 109°$. The inferred magnetic field direction on intermediate scales is therefore aligned within a few degrees of the mean jet direction ($\theta \simeq 200°$).

0954+658 = 4C 55.17.—The source is identified with a BL Lacertae object to which Lawrence et al. (1986) ascribe a tentative redshift of $z = 0.368$ (1 mas = 3.1 h^{-1} pc). It exhibits intraday radio variability (Witzel 1990), and extreme interstellar scattering, or "Fiedler events" (Fiedler et al. 1987; Romani, Blandford, & Cordes 1987). The *I* and *P* images of this source have been discussed by GCRW92 and are reproduced in Figures 7*a*–7*c*. Flux and polarization measurements at the VLA showed that the source did not vary significantly during our observations.

© American Astronomical Society • Provided by the NASA Astrophysics Data System

1993ApJ...416..496C

The I image shows a "core-jet" structure. The jet has an initial position angle $\theta \simeq -70°$ and then curves slightly to the north. The P image shows two distinct components of strong and nearly orthogonal polarization. The plane of the electric field of polarization in the "jet" makes an angle of 34° with the direction of displacement between the two polarized components, which is larger than is typical for BL Lacertae objects (GCRW92). If the component positions listed in Table 4 are taken at face value, then the jet is possibly quite twisted. The local jet direction at the position of K2 may be closer to $\theta = 90°$, in which case the E vectors would be aligned within 14° of the jet.

No image of this source was published by PR88. Zensus, Porcas, & Pauliny-Toth (1984) fitted an elliptical Gaussian model oriented at position angle $\theta = -54°$, based on observations with only three antennas. Using the VLA at 1.6 GHz, Rusk (1988) observed a curved jet of length 4″ at a mean position angle $\theta = -153°$ (see also Perley 1982). The jet therefore bends through $\sim 90°$ between milliarcsecond and arcsecond scales.

1624+416 = DA 411 = 4C 41.32.—This source is identified with a 22 mag quasar of redshift $z = 2.55$. VLA measurements at the time of our observations placed an upper limit of 1.5 mJy on any linearly polarized flux from this source. The P image showed no feature brighter than 3 mJy. The I image was consistent with that by PR88, who find a jet that emerges to the west and subsequently veers to the south. Using the VLA at 5 GHz, Rusk (1988) observed a short extension of length 0.″7 at position angle $\theta = -8°$ (see also Perley 1982; O'Dea et al. 1988), indicating extreme bending between milliarcsecond and arcsecond scales. The absence of any linearly polarized flux makes 1624+416 one of only two unpolarized quasars in this sample (the other being 0153+744), and we show neither the I nor the P image here.

1633+382 = 4C 38.41.—This is an 18 mag quasar with a redshift $z = 1.814$ (1 mas = 4.2 h^{-1} pc). The I and P images (Figs. 8*a*–8*c*) show a bright, weakly polarized component with faint extensions to the northwest and southwest that are visible in I only. Fitting to the visibility data yields the three-component model shown in Table 4. We detect polarized flux only in the brightest component, presumably the core. The core is strong enough that the parameters for the jet components are not well constrained, but both the model and the image suggest that the jet has an initial position angle $\theta \simeq -45°$ and bends sharply to the southwest. VLA observations at 5 GHz by Rusk (1988) show a jet of length 2″ at position angle $\theta = 176°$, apparently continuing this trend.

The observations of this source by PR88 were made in 1979 April. At that epoch they found a 0.8 Jy component with two fainter components, each of approximately 0.4 Jy, 0.3 and 1.4 mas distant, both at position angle $\theta = -64°$. Because of the large time interval (5.5 yr) between the two observations, it is not clear how to relate features on the two images. Their image is quite similar to ours, and also suggests bending of the jet. The core component brightened by a factor of 2.7 over this period, consistent with the rapid variability observed by Seielstad et al. (1983).

1641+399 = 3C 345.—This celebrated superluminal quasar ($z = 0.595$; 1 mas = 3.8 h^{-1} pc) has been observed many times by us and by others (in particular, in total intensity, by the Caltech group; see Biretta, Moore, & Cohen 1986 and references therein). We have monitored the milliarcsecond polarization structure at 5 GHz since 1981 (Wardle et al. 1986, 1988; Brown et al. 1993). In Figures 9*a*–9*c* we show I and P images made from data taken in 1984 March. In Table 4 we use the component names adopted by the Caltech group.

A detailed discussion of the polarization of this source and its evolution is given in Brown et al. (1993). The core (component D) is weakly polarized ($m \simeq 2.0\%$), and the degree of polarization increases down the jet. The inferred magnetic field direction in the most strongly polarized component, C3, is closely aligned with the local jet direction. Component C2 is clearly resolved, and the polarization is mainly at the southwestern edge. Its polarization angle is inclined at about 30° to the direction of the jet, and may indicate an oblique shock.

Deep VLA observations at 5 GHz (Kollgaard, Wardle, & Roberts 1989) show a straight jet extending 3″ at position angle $\theta = -61°$, embedded in more diffuse emission with an overall extent of some 20″. The structure on intermediate scales contains 103 mJy of polarized flux ($m \simeq 5\%$) at position angle $\chi = 53°$. Thus the magnetic field appears to be roughly parallel to the jet on scales between 10 mas and 1″.

1652+398 = Mrk 501 = DA 426 = 4C 39.49.—This source is identified with a 14 mag elliptical galaxy of redshift $z = 0.0337$ (1 mas = 0.46 h^{-1} pc) having a bright (but low-luminosity) nonthermal nucleus, and is often listed as a BL Lacertae object (Burbidge & Hewitt 1987). Ulrich et al. (1975) consider it to be an intermediate object between ordinary elliptical and BL Lacertae objects. Maza, Martin, & Angel (1978) call it a "mini–BL Lac object." At centimeter radio wavelengths, this source is barely variable in total intensity and only somewhat so in polarization (Aller et al. 1985). At optical wavelengths it is modestly polarized (2%–4%) and exhibits a preferred polarization position angle in the range 125°–145° (Angel & Stockman 1980).

Our observations of this source were discussed in GCRW92. Although our VLA measurements of the source polarization indicate the presence of 26 mJy of polarized flux somewhere in the VLA core, no polarized feature brighter than ~ 4 mJy was found on the resulting P image. Hence only the I image is shown here (Fig. 10). This shows a nearly continuous jet at position angle $\sim 140°$, and is very similar to the image in PR88, made from data taken in 1980.53. Their inner knot is coincident within the uncertainties with our K2. If it is the same knot, then it is stationary. If it should be identified with our K1, then it has a subluminal velocity of $\beta_{\rm app} \simeq 0.4\,h^{-1}$.

Van Breugel & Schilizzi (1986) have made 5 GHz observations using the European VLBI Network (EVN), and show that the jet continues at least 55 mas from the core at an initial position angle of $\theta \simeq 130°$, and curves slightly to the north. If the polarized flux seen by the VLA, but absent from our image, is attributed to this larger scale jet, then its fractional polarization is $m \geq 4\%$ at $\chi = 136°$. Thus the electric vectors may well be roughly aligned with the jet direction, as we find in other BL Lacertae objects (GCRW92). If Mrk 501 were at a more typical redshift of, say, $z \simeq 0.3$, then the polarized part of the jet would be only ~ 5 mas from the core, and it would be easily imaged by our observations (of course the source would not then be in the sample!). Thus, the polarization of the jet may resemble that of more luminous BL Lacertae objects, but the core polarization is certainly anomalously low (see Paper II and GCRW92) and is more typical of the other sources identified with normal galaxies in this sample.

VLA observations by Ulvestad, Johnston, & Weiler (1983) show very diffuse emission over about 1′, elongated along position angle $\theta = 45°$, almost orthogonal to the jet on milliarcsecond scales.

1749+701.—This is a BL Lacertae object to which Stickel,

© American Astronomical Society • Provided by the NASA Astrophysics Data System

1993ApJ...416..496C

Fried, & Kühr (1988) assign a tentative redshift of $z = 0.77$ (1 mas = 4.1 h^{-1} pc) based on a single emission line. A similar redshift was suggested by Arp et al. (1976), and is confirmed by C. R. Lawrence (1992, private communication). Our observations of this source were discussed previously in GCRW92. Although polarization measurements made at the VLA during these observations indicate the presence of ~ 14 mJy of polarized flux somewhere within the VLA core, less than ~ 4 mJy is found in the VLBI image.

The total intensity image (Fig. 11) shows a bright core and a jet (modeled as three knots) extending to the northwest at position angle $\theta \simeq -60°$; there is some indication that the jet may curve toward the north at large distances from the core. The model in Table 4 provides a good fit to the I data.

If the knot labeled K2 is the same knot detected by PR88 in observations made in 1980.74, a proper motion of $\mu \simeq 0.15$ mas yr^{-1} is indicated. Witzel et al. (1988) obtained a similar result (0.1 mas yr^{-1}) by comparing their 5 GHz image at epoch 1985.8 with images from 1981–1982 by Bååth (1984). Since neither set of fits is published, it is not possible to combine their results with ours and those of PR88. This source is mildly superluminal with $\beta_{app} \simeq 3\,h^{-1}$.

VLA observations (O'Dea et al. 1988; Rusk 1988) at 15 GHz show a single secondary component 0".4 southwest of the core at position angle $\theta \simeq -153°$. At 5 GHz, Rusk's image indicates a small extension to the northwest. The intermediate-scale structure contains 170 mJy of I flux. Its polarized flux density is 14 mJy ($m \simeq 8\%$) at position angle $\chi = 108°$. This polarization should be reliable, since it is essentially the value measured directly at the VLA. The electric vector is therefore aligned within 19° of the direction of the milliarcsecond jet at the position of the outer component K1.

Our observations of 1749+701 are reminiscent of those of 1652+398 (above). The I images are very similar, showing no significant polarization on milliarcsecond scales, in striking contrast to all the other BL Lacertae objects we have observed. Both have significantly polarized intermediate scale structure, with the electric vector roughly parallel to the VLBI jet. However, other properties of these sources are quite different. At $z = 0.770$, 1749+701 is a high luminosity object. At radio wavelengths it is extremely variable on all time scales (Witzel 1990; Seielstad et al. 1983; Aller et al. 1985), and at optical wavelengths it exhibits strong and variable polarization (Wills et al. 1980; Impey & Tapia 1990). In addition, 1652+398 shows relatively prominent optical line emission, while the spectrum of 1749+701 is nearly featureless (Impey, Lawrence, & Tapia 1991).

1803+784.—This is a BL Lacertae object with a redshift of $z = 0.68$ (1 mas = 4.0 h^{-1} pc) and particularly luminous emission lines (Lawrence 1990). This source has been imaged by PR88 and several times by Witzel et al. (1988). Both groups modeled the source as a double, with a constant separation ~ 1.2 mas, leading to a subluminal velocity of $\beta_{app} < 0.74\,h^{-1}$.

Images made from data taken in 1987 May were discussed in GCRW92 and are reproduced in Figures 12*a*–12*c*. The dominant structure is that of a polarized double, with electric vectors in both components roughly parallel to the direction of their separation ($\theta = 96°$). The polarization position angles are corrected for $-15°$ of Faraday rotation. A significantly better fit to the data was obtained with the triple model in Table 4 than with a model including only the two strongest components. The inner knot, K1, would appear to be the same component observed by PR88 and by Witzel et al. If so, it has persisted and remained nearly stationary for almost 10 years. This is somewhat surprising, since 1803+784 is a rapid optical and radio variable (Witzel 1990).

Krichbaum (1990) shows a VLBI image made at 43 GHz. This shows that the jet is strongly bent on submilliarcsecond scales. VLA observations by Antonucci et al. (1986) show a 2" extension at position angle $\theta \simeq -120°$, and also a component 45" distant at position angle $\theta \simeq -166°$, which is presumably related. This source has 43 mJy of polarized flux on intermediate scales in position angle $\chi = 78°$. Thus the electric vector is roughly parallel to both the milliarcsecond-scale jet and the arcsecond extension.

1807+698 = 3C 371.—In the literature this object has been described variously as an N galaxy or as a BL Lacertae object in the center of an elliptical galaxy (Miller, French, & Hawley 1978; Miller 1975, 1981). It has an emission-line redshift of $z = 0.050$ (1 mas = 0.67 h^{-1} pc).

The I and P images were discussed by GCRW89 and are reproduced in Figures 13*a*–13*c*. The I image shows the well-known jet structure that has been imaged by PR88 and more extensively by Lind (1987), who finds collimated structure out to 30 mas from the core at position angle $\theta \simeq -100°$. Our image (made from more poorly sampled data) follows the jet for only about 7 mas. The jet appears to have a continuous distribution of flux, and attempts to fit discrete components to this source were unsuccessful. We detect no polarization from the core ($m < 0.5\%$) and only ~ 7 mJy of polarized flux in the jet close to Lind's knot A ($m > 20\%$). However, the VLA recorded some 40 mJy of linearly polarized flux from the arcsecond core during these observations, so that 30–35 mJy of polarized flux lies between the scales accessible to the VLA and those of the image shown here. The rotation measure of the VLA core has been measured to be $+339 \pm 24$ rad m^{-2} (Wrobel 1987; O'Dea 1989). This therefore applies to these intermediate scales (where most of the polarized flux at this wavelength resides) rather than to the milliarcsecond scales of our observations, and so the intrinsic polarization angle of the polarized feature we detect remains unknown. Applying this rotation measure to the intermediate-scale polarized flux, we find that the electric vector has a position angle of $\chi = 168°$, almost precisely perpendicular to the direction of the jet, implying a longitudinal magnetic field.

Deep VLA observations by Wrobel & Lind (1990) show twin radio lobes, a one-sided jet, and a hot spot, characteristic of Fanaroff-Riley Type II (FR II) radio sources. The intermediate-scale polarization that we find is consistent with this.

1823+568 = 4C 56.27.—This is a BL Lacertae object with a redshift of $z = 0.664$ (1 mas = 3.9 h^{-1} pc). The I and P images shown in Figures 14*a*–14*c* were discussed by GCRW89. Both images show a core-jet structure along position angle $\theta \simeq 190°$. The three–point-component model given in Table 4 proved to be a good fit to the data. The polarization position angles of the two southern components are close to the orientation of the jet.

The image published by PR88 is qualitatively similar to ours, although both the core and the jet have faded considerably since their observations (epoch 1979.92). PR88 obtain a good fit with a two-component model. If their southern component is the same as our K1, then the proper motion is $\mu \simeq 0.12$ mas yr^{-1}, corresponding to $\beta_{app} \simeq 2.5\ h^{-1}$ (GCRW89).

VLA observations (O'Dea et al. 1988; Rusk 1988) show a jet

© American Astronomical Society • Provided by the NASA Astrophysics Data System

1993ApJ...416..496C

extending about 1″ at position angle $\theta = -175°$ that bends to the northeast through some 120° to form a lobe at position angle $\theta = 95°$. The jet appears to have a longitudinal magnetic field. Although there is appreciable I flux on intermediate scales (370 mJy), there is no significant P flux (≤ 6 mJy).

1828+487 = 3C 380.—This is a high-luminosity "compact steep-spectrum" quasar with a redshift of $z = 0.692$ (1 mas = 4.0 h^{-1} pc). On milliarcsecond scales it shows a complex structure consisting of a core and a twisting jet (Wilkinson et al. 1984, 1990; PR88). Our I and P images are shown in Figures 15*a*–15*c*. Despite the rather sparse u-v coverage for such a complex source, the I structure shown here is in good agreement with that found by Wilkinson et al. and by PR88.

To the southeast is an unresolved core component, which is less than 1% polarized. Some 6 mas distant at position angle $\theta = -31°$ is a bright knot (our K3) that is approximately 4% polarized. The peak of polarized intensity in the knot appears to be displaced significantly westward from the peak in total intensity. At this knot the local jet direction changes to $\theta = -70°$. About 3.3 mas from this knot lies another, fainter feature (K2) that is extended in the north-south direction. This is coincident with the peak in polarized intensity, and the degree of polarization is nominally 77%. The uncertainty associated with this value stems not from the signal-to-noise ratio of the P image but from the fidelity of the I image, which is faint and extended at this location. There is no doubt that the degree of polarization is close to the maximum permitted from incoherent synchrotron radiation, indicating an extremely well-ordered magnetic field. This high polarization is confirmed in new observations (Cawthorne 1993). The VLBI structure detected in these observations terminates in an extended component (K1), the peak of which is significantly set back from the leading edge. The polarized flux of this component seems to be confined to its eastern and northern boundaries.

By comparing images made in 1982.94 and 1988.44, Wilkinson et al. (1990) infer velocities $\beta_{app} \simeq 2.6\ h^{-1}$ in a nonradial direction (position angle $\sim 20°$) for our component K3, and $\beta_{app} \simeq 8\ h^{-1}$ for our component K1. Our observations were made between their epochs, but do not appear to support their result. The outer component K1 is extended and complex, and it is difficult to assign an accurate position. K3 is also embedded in extended emission, and Wilkinson et al. noted that it had brightened by a factor of 4 between their epochs. It is possible that both apparent proper motions are instead due to changes in the brightness distribution. Wilkinson et al. also make the intriguing suggestion that K3 may be a second nucleus. While we can neither support this nor rule it out, we note that this knot's fractional polarization (4%) is more than twice that of any other quasar core we have observed (e.g., Roberts et al. 1990b; Paper II). Its polarization properties seem more consistent with those of a knot in a bent jet.

Although the polarization structure is complex, the directions of the electric field vectors are remarkably uniform, as was noted in the case of 0836+710. However, unlike 0836+710, the position angle of polarization, $\chi = 16°$, at the most strongly polarized feature, K2, implies a projected magnetic field that lies within 4° of the *local* jet direction, $\theta = -70°$. The electric vectors have been corrected for +27° of Faraday rotation (RM = 130 ± 5 rad m^{-2}; Wilkinson et al. 1991). If this derotation is correct on milliarcsecond scales, then the alignment of the magnetic field with the local jet direction beyond K3 rather than with the radial displacement from the core appears to support the idea that the structure of the jet delineates the flow of material, rather than being the locus of components moving out of the core "ballistically" (along radial paths).

The uniformity of the field direction contrasts strikingly with the complex and irregular nature of the jet in both total intensity and polarized intensity. This might be taken to imply that underlying this complex structure the flow possesses significant uniformity. The jet could be a broad and uniform flow with a longitudinal magnetic field, the bright features merely representing places where the flow is disturbed. Such a view was suggested on theoretical grounds by Blandford (1984).

Wilkinson et al. (1991) show several images of 3C 380 made with MERLIN and the VLA. On arcsecond scales, the jet emerges from the core at position angle $\theta = -47°$, terminating in what may be classical hot spots. This structure is embedded in complex diffuse emission about 15″ in extent. Unfortunately, our VLA measurements of 3C 380 were not preserved. It is certain that substantial quantities of flux are missing from the images shown here. This source is only weakly variable at centimeter wavelengths (Seielstad et al. 1983). VLA observations by Rusk (1988) 3 months after our observations show a core flux density of 2470 mJy, with a polarized flux of 168 mJy at position angle $\chi = 40°$. This suggests that the intermediate-scale structure is significantly polarized ($m \simeq 8\%$) and that the magnetic field continues to run parallel to the jet.

1928+738 = 4C 73.18.—This is a 16.5 mag quasar with a redshift of $z = 0.302$ (1 mas = 2.8 h^{-1} pc). It shows significant intraday variability at centimeter wavelengths (Witzel 1990). PR88 classify the VLBI structure as "asymmetric I." Their image shows a bright core and a jet pointing south, which they model as four knots. The Bonn group has imaged this source at several epochs (Eckart et al. 1985, 1987; Witzel et al. 1988). They find a complex jet, about 20 mas in length, in which they identify as many as nine components. At least five of these exhibit superluminal motion, with $\beta_{app}h$ in the range 4.7–6.9.

Our images also show a complicated structure, and are shown in Figures 16*a*–16*c*. Because the u-v plane was undersampled in these observations, we only show the inner 14 mas of the images. There is clearly emission farther to the south, but we are not confident that the features we see are reliable.

The bright core (which has faded by ~ 1 Jy since the observations by PR88 in 1980.72) is approximately 1% polarized. The innermost knot, K4, is blended with the core in I but more distinct in P, since it is much more strongly polarized ($\sim 8\%$). The next component (K3) appears to be resolved laterally in polarization and is $\sim 10\%$ polarized. K3 and K4 are clearly the same as the components labeled "C2" and "C3," respectively, in Witzel et al. (1988). The region between 8 and 12 mas south of the core is resolved and complex (see also the epoch 1984.79 image in Witzel et al. 1988), and division into distinct components is somewhat arbitrary. The components K1 and K2 listed in Table 4 correspond to the two peaks in the I image (and also, roughly, to C6 and C7 in Witzel et al. 1988). The peaks in polarized intensity are displaced significantly to the north of the I peaks. The average degree of polarization in this region is at least 10%.

The position angle of the electric vectors increases down the jet, from $\chi = 29°$ in K4 to $\chi = 88°$ in K1/K2. Thus the apparent magnetic field direction is misaligned with the local direction of the jet by 34° in the inner knot, K4, but it becomes roughly parallel further downstream. Similar behavior has

© American Astronomical Society • Provided by the NASA Astrophysics Data System

1993ApJ...416..496C

been seen in other quasars with complex jets (e.g., 3C 273: Roberts et al. 1990a; 3C 345: Brown et al. 1993).

VLA observations (Johnston et al. 1987; Kollgaard et al. 1990) show extended ($\sim 90''$) emission with many of the characteristics of a classical FR II radio source. A conspicuous jet with a longitudinal magnetic field emerges from the VLA core at position angle $\theta = 190°$ and then bends to the southeast, terminating in a hot spot. This is presumably the continuation of the VLBI jet. An unusual feature is that there appears to be a counterjet emerging to the north. Lawrence (1990) also reports the detection of extended [O III] $\lambda 5007$ emission in the region north of the optical nucleus. The polarized flux on intermediate scales is $p \simeq 68$ mJy ($m \simeq 17\%$) at position angle $\chi \simeq 112°$, so the magnetic field appears to be nearly parallel to the initial direction of the jet on arcsecond scales.

2021+614 = OW 637.—This source is identified with a 19.5 mag galaxy with a redshift of $z = 0.227$. It is essentially unpolarized at both optical and radio wavelengths (Impey & Tapia 1990; Perley 1982). VLBI observations made in 1984 March produced an *I* image consistent with that by PR88, showing two components, each of which is resolved into two subcomponents (see also Bartel et al. 1984). No polarized flux greater than 5 mJy was detected by the VLA, or in our VLBI image, and we show no images of this object.

2200+420 = BL Lac.—This prototypical object lies at the center of a giant elliptical galaxy with weak emission lines at $z_{gal} = 0.069$ (1 mas = 0.90 h^{-1} pc). It is violently variable and strongly polarized in all wave bands (Angel & Stockman 1980). A detailed sequence of VLBI total intensity images have been published by Mutel et al. (1990). Their 10.7 GHz observations show a stationary core and a series of knots moving in a southerly direction with a superluminal speed of $\beta_{app} \simeq 3.5$ h^{-1}. The integrated flux and polarization behavior at three wavelengths has been modeled in detail by Hughes, Aller, & Aller (1985, 1989). They describe the moving knots as plane-parallel shocks that compress the underlying (tangled) magnetic field in the jet into a plane perpendicular to the jet.

We have observed this source several times. In Figures 17*a*–17*c* we show images made from data taken in 1984 March, published previously in GCRW89. The polarization position angles are corrected for $-42°$ of Faraday rotation (RM = -205 ± 5 rad m^{-2}; Rudnick et al. 1984). Although the images give the impression of a rather smooth distribution of emission, the signal-to-noise ratio and the *u-v* coverage of these observations permit quite detailed model fitting. In Table 4 we give a four-component fit to the data that supersedes the three-component model given in GCRW89.

The brightest feature in our images is the inner knot (K3) rather than the core. This is undoubtedly the component S3 in the sequence of images by Mutel et al. (1990). Our knots K2 and K1 probably correspond to their S2 and S1, which are no longer visible on their 10.7 GHz images near the epoch of our observations, presumably due to resolution. These knots define a jet that initially points nearly due south and then turns slightly to the east, as first noted by Mutel et al. (1990). The knot K3 is presumably the component modeled in detail by Hughes et al. (1985, 1989), which corresponds to the polarized outburst which peaked in mid-1983. The component had weakened sufficiently by the epoch of these observations that we cannot compare our results in detail to their model, but the accurate alignment of the polarization position angle with the direction of the jet offers considerable support.

The total polarized flux found in the VLBI image is greater than that observed with the VLA. This implies that the intermediate-scale polarized flux is nearly orthogonal to the milliarcsecond-scale polarized flux ($p_{int} = 25$ mJy at $\chi = 82°$). Lower resolution (EVN or MERLIN) images would be of great interest, to see whether the milliarcsecond-scale jet turns farther to the east, or whether it continues in a mainly southerly direction. Deep observations at arcsecond resolution with the VLA (Ulvestad & Johnston 1984; Antonucci 1986) reveal very faint emission surrounding the bright core, with an angular extent of about 30″ oriented at position angle $\sim 130°$. Observations with the Westerbork Synthesis Radio Telescope (WSRT) (de Bruyn & Schilizzi 1984) also show diffuse emission, but with a different orientation. In any case, the extended structure is too amorphous to reveal the path of the jet on arcsecond scales.

2351+456 = 4C 45.51 = OZ 486.—This faint (20.6 mag) object has been identified as a high-redshift quasar ($z = 2.0$; unpublished work by C. R. Lawrence & S. C. Uwin, quoted by PR88; 1 mas = 4.1 h^{-1} pc). It is modestly variable on a time scale of months at 10.7 GHz (Seielstad et al. 1983).

Figures 18*a*–18*c* show the *I* and *P* images. The *I* image is qualitatively similar to that by PR88 (epoch 1980.53). The source consists of a compact component in the east, a resolved knot about 3.5 mas distant at position angle $\theta = 70°$, and some more diffuse emission to the west. PR88 found three components: the core, an inner knot 1.6 mas distant at a similar position angle to that of the "jet" component in the images shown here, and a further component 3.9 mas from the core. Apparently, either their inner knot faded in the intervening 4 years (in which case the outer knot appears to be stationary), or both moved outward so that by 1984 the innermost knot on the 1980 image had reached the position of the knot on our image (suggesting the high value $\beta_{app} \simeq 20\, h^{-1}$).

No correction for Faraday rotation has been applied to the polarization position angles. Rusk (1988) gives RM = -12 rad m^{-2} but indicates that this value is not reliable, since the source is almost unpolarized at L band. While the low polarization of the core (1.2%) is typical of quasars (see Paper II and Roberts et al. 1990b), the polarization position angle of the knot is aligned within 22° of the structural position angle. Such an orientation is more typical of BL Lacertae objects, although, since the rotation measure is not known, this may be misleading.

VLA observations by Rusk (1988) suggest an extremely bent jet that emerges from the VLA core at position angle $\theta \simeq 25°$ and bends sharply to the northwest after about 0.″4. Although there is ~ 490 mJy (in *I*) on intermediate scales, there is apparently no significant polarized flux ($p \leq 2$ mJy).

2352+495 = OZ 488.—This object is identified with a 19 mag elliptical galaxy of redshift $z = 0.237$. The *I* image made from data taken in 1984 October shows a bright feature with faint extensions to the north and south, very similar to the southern feature in the image by PR88. Because of the poor sampling of short *u-v* spacings, the weak feature that they found ~ 17 mas north was not detected. Conway et al. (1990) have found a third component, weaker still, ~ 12 mas south of the bright feature. No polarized flux in excess of 3 mJy was found on the *P* image. VLA measurements made during the observations reveal only 2 mJy of polarized flux. Almost 50% of the *I* flux observed at the VLA during these observations is missing from the image, indicating that there is significant flux on intermediate scales. Perley (1982) found no extended structure on scales larger than 0.″2. Because of our poor *u-v* coverage

© American Astronomical Society • Provided by the NASA Astrophysics Data System

1993ApJ...416..496C

and the lack of polarization, we do not show images of this source.

4. CONCLUSIONS

We have presented polarization-sensitive VLBI observations at 5 GHz of 24 sources from the Pearson-Readhead complete sample. Sixteen sources showed detectable polarization on milliarcsecond scales, and we have shown both total intensity and polarization images of these, and total intensity images of two additional BL Lacertae objects. These observations have demonstrated the ability of a global VLBI array to make polarization images from relatively short "snapshots" of data. The polarization images display a rich variety of properties. The fractional polarization of individual components ranges from below the limit of detection ($m \lesssim 0.5\%$) up to the theoretical maximum for incoherent synchrotron radiation in a uniform magnetic field ($m \simeq 70\%$). A detailed discussion of these results is presented in Paper II.

The authors thank the staff of the Haystack Mark III correlator and of all the participating observatories for their help in recording and reducing the data presented here. We are grateful to Tim Pearson for his constructive comments on the manuscript, and to George Moellenbrock for his help in producing the final images. This work was supported by the National Science Foundation under grants AST 84-18636 and AST 88-01743 (J. F. C. W.) and AST 85-19529, AST 88-22718, and AST 91-22282 (D. H. R.), and also by the Smithsonian Institution. Observations at the US VLBI network stations and astronomy operations of the Haystack Mark III correlator are also supported by the National Science Foundation. The National Radio Astronomy Observatory is operated by Associated Universities, Inc., under a cooperative agreement with the National Science Foundation.

REFERENCES

Aller, H. D., Aller, M. F., Latimer, G. E., & Hodge, P. E. 1985, ApJS, 59, 513
Altschuler, D. R., & Wardle, J. F. C. 1976, MemRAS, 82, 1
Angel, J. R. P., & Stockman, H. S. 1980, ARA&A, 18, 321
Antonucci, R. R. J. 1986, ApJ, 304, 634
Antonucci, R. R. J., Hickson, P., Olszewski, E. W., & Miller, J. S. 1986, AJ, 92, 1
Arp, H. C., Sulentic, J. W., Willis, A. G., & de Ruiter, H. R. 1976, ApJ, 207, L13
Bååth, L. 1984, in IAU Symp. 110, VLBI and Compact Radio Sources, ed. R. Fanti, K. Kellermann, & G. Setti (Dordrecht: Reidel), 127
Bartel, N., et al. 1984, ApJ, 279, 116
Baum, S. A., O'Dea, C. P., Murphy, D. W., & de Bruyn, A. G. 1990, A&A, 232, 19
Biretta, J. A., Moore, R. L., & Cohen, M. H. 1986, ApJ, 308, 93
Blandford, R. D. 1984, in IAU Symp. 110, VLBI and Compact Radio Sources, ed. R. Fanti, K. Kellermann, & G. Setti (Dordrecht: Reidel), 215
Brown, L. F., Roberts, D. H., & Wardle, J. F. C. 1993, in preparation
Burbidge, G. R., & Hewitt, A. 1987, AJ, 93, 1
Cawthorne, T. V. 1993, in preparation
Cawthorne, T. V., Wardle, J. F. C., Roberts, D. H., & Gabuzda, D. C. 1993, ApJ, 416, 519 (Paper II)
Conway, J. E., Pearson, T. J., Readhead, A. C. S., & Unwin, S. C. 1990, in Superluminal Radio Sources, ed. J. A. Zensus & T. J. Pearson (Cambridge: Cambridge Univ. Press), 167
de Bruyn, A. G., & Schilizzi, R. T. 1984, in IAU Symp. 110, VLBI and Compact Radio Sources, ed. R. Fanti, K. Kellermann, & G. Setti (Dordrecht: Reidel), 165
Eckart, A., Witzel, A., Biermann, P., Johnston, K. J., Simon, R., Schalinski, C., & Kühr, H. 1986, A&A, 168, 17
———. 1987, A&AS, 67, 121
Eckart, A., Witzel, A., Biermann, P., Pearson, T. J., Readhead, A. C. S., & Johnston, K. J. 1985, ApJ, 296, L23
Fiedler, R. L., Dennison, B., Johnston, K. J., & Hewish, A. 1987, Nature, 326, 675
Gabuzda, D. C., Cawthorne, T. V., Roberts, D. H., & Wardle, J. F. C. 1989a, ApJ, 347, 701 (GCRW89a)
———. 1992, ApJ, 388, 40 (GCRW92)
Gabuzda, D. C., Wardle, J. F. C., & Roberts, D. H. 1989b, ApJ, 338, 743
Hughes, P. A., Aller, H. D., & Aller, M. F. 1985, ApJ, 298, 310
———. 1989, ApJ, 341, 68
Hummel, C. A., Muxlow, T. W. B., Krichbaum, T. P., Quirrenbach, A., Schalinski, C. J., Witzel, A., & Johnston, K. J. 1992, A&A, 266, 93
Hummel, C. A., Schalinski, C. J., Krichbaum, T. P., Witzel, A., & Johnston, K. J. 1988, A&A, 204, 68
Impey, C. D., Lawrence, C. R., & Tapia, S. 1991, ApJ, 375, 46
Impey, C. D., & Tapia, S. 1990, ApJ, 354, 124
Johnston, K. J., Simon, R. S., Eckart, A., Biermann, P., Schalinski, C., Witzel, A., & Strom, R. G. 1987, ApJ, 313, L85
Kollgaard, R. I., Wardle, J. F. C., & Roberts, D. H. 1989, AJ, 97, 1550
———. 1990, AJ, 100, 1057
Krichbaum, T. P. 1990, in Parsec-Scale Radio Jets, ed. J. A. Zensus & T. J. Pearson (Cambridge: Cambridge Univ. Press), 83
Krichbaum, T. P., Hummel, C. A., Quirrenbach, A., Schalinski, C. J., Witzel, A., Johnston, K., Muxlow, T. W. B., & Qian, S. J. 1990, A&A, 230, 271
Lawrence, C. R. 1990, in Parsec-Scale Radio Jets, ed. J. A. Zensus & T. J. Pearson (Cambridge: Cambridge Univ. Press), 280
Lawrence, C. R., Pearson, T. J., Readhead, A. C. S., & Unwin, S. C. 1986, AJ, 91, 494
Lind, K. R. 1987, in Superluminal Radio Sources, ed. J. A. Zensus, & T. J. Pearson (Cambridge: Cambridge Univ. Press), 180
Marr, J. M., Backer, D. C., & Wright, M. C. H. 1990, in Parsec-Scale Radio Jets, ed. J. A. Zensus & T. J. Pearson (Cambridge: Cambridge Univ. Press), 78
Maza, J., Martin, P. G., & Angel, J. R. P. 1978, ApJ, 224, 368
Miller, J. S. 1975, ApJ, 200, L55
———. 1981, PASP, 93, 681
Miller, J. S., French, H. B., & Hawley, S. A. 1978, in Pittsburgh Conf. on BL Lac Objects, ed. A. Wolfe (Pittsburgh: Univ. Pittsburgh), 176
Mutel, R. L., Phillips, R. B., Su, B., & Bucciferro, R. R. 1990, ApJ, 352, 81
O'Dea, C. P. 1989, A&A, 210, 35
O'Dea, C. P., Barvainis, R., & Challis, P. M. 1988, AJ, 96, 435
Pearson, T. J., & Readhead, A. C. S. 1984, in IAU Symp. 110, VLBI and Compact Radio Sources, ed. R. Fanti, K. Kellermann, & G. Setti (Dordrecht: Reidel), 15
———. 1988, ApJ, 328, 114 (PR88)
Perley, R. A. 1982, AJ, 87, 859
Readhead, A. C. S., Pearson, T. J., & Unwin, S. C. 1984, in IAU Symp. 110, VLBI and Compact Radio Sources, ed. R. Fanti, K. Kellermann, & G. Setti (Dordrecht: Reidel), 131
Readhead, A. C. S., Venturi, T., Marr, J. M., & Backer, D. C. 1990, in Parsec-Scale Radio Jets, ed. J. A. Zensus & T. J. Pearson (Cambridge: Cambridge Univ. Press), 71
Roberts, D. H., Brown, L. F., & Wardle, J. F. C. 1991, in IAU Colloq. 131, Radio Interferometry: Theory, Techniques, and Applications, ed. T. J. Cornwell & R. A. Perley (San Francisco: ASP), 281
Roberts, D. H., Gabuzda, D. C., & Wardle, J. F. C. 1987, ApJ, 323, 536
Roberts, D. H., Kollgaard, R. I., Gabuzda, D. C., Brown, L. F., & Wardle, J. F. C. 1990a, ApJ, 360, 408
Roberts, D. H., Potash, R. I., Wardle, J. F. C., Rogers, A. E. E., & Burke, B. F. 1984, in IAU Symp. 110, VLBI and Compact Radio Sources, ed. R. Fanti, K. Kellermann, & G. Setti (Dordrecht: Reidel), 35
Roberts, D. H., Wardle, J. F. C., & Brown, L. F. 1993, ApJ, submitted
Roberts, D. H., Wardle, J. F. C., Brown, L. F., Gabuzda, D. C., & Cawthorne, T. V. 1990b, in Parsec-Scale Radio Jets, ed. J. A. Zensus & T. J. Pearson (Cambridge: Cambridge Univ. Press), 110
Romani, R. W., Blandford, R. D., & Cordes, J. M. 1987, Nature, 328, 324
Rudnick, L., Jones, T. W., Edgar, B. K., & Pedelty, J. A. 1984, AJ, 89, 316
Rusk, R. 1988, Ph.D. thesis, Univ. Toronto
Scheuer, P. A. G. 1987, in Astrophysical Jets and Their Engines, ed. W. Kundt (Dordrecht: Reidel), 137
Seielstad, G. A., Pearson, T. J., & Readhead, A. C. S. 1983, PASP, 95, 842
Stickel, M., Fried, J. W., & Kühr, H. 1988, A&A, 198, L13
Ulrich, M.-H., Kinman, T. D., Lynds, C. R., Rieke, G. H., & Ekers, R. D. 1975, ApJ, 198, 261
Ulvestad, J. S., & Johnston, K. J. 1984, AJ, 89, 189
Ulvestad, J. S., Johnston, K. J., & Weiler, K. W. 1983, ApJ, 266, 18
van Breugel, W., & Schilizzi, R. 1986, ApJ, 301, 834
Wardle, J. F. C., & Kronberg, P. P. 1974, ApJ, 194, 249
Wardle, J. F. C., & Roberts, D. H. 1986, Canadian J. Phys., 64, 353
Wardle, J. F. C., Roberts, D. H., Brown, L. F., & Gabuzda, D. C. 1988, in IAU Symp. 129, The Impact of VLBI on Astrophysics and Geophysics, ed. M. J. Reid & J. M. Moran (Dordrecht: Reidel), 163
Wardle, J. F. C., Roberts, D. H., Potash, R. I., & Rogers, A. E. E. 1986, ApJ, 304, L1

© American Astronomical Society • Provided by the NASA Astrophysics Data System

1993ApJ...416..496C

Wilkinson, P. N., Akujor, C. E., Cornwell, T. J., & Sakia, D. J. 1991, MNRAS, 248, 86
Wilkinson, P. N., Cornwell, T. J., Kus, A. J., Readhead, A. C. S., & Pearson, T. J. 1984, in Physics of Energy Transport in Extragalactic Radio Sources, ed. A. H. Bridle & J. A. Eilek (Green Bank: NRAO), 76
Wilkinson, P. N., Tzioumis, A. K., Akujor, C. E., Benson, J. M., Walker, R. C., & Simon, R. S. 1990, in Parsec-Scale Radio Jets, ed. J. A. Zensus & T. J. Pearson (Cambridge: Cambridge Univ. Press), 152
Wills, D., Wills, B. J., Breger, B., & Hsu, J.-C. 1980, AJ, 85, 1555
Witzel, A. 1990, in Parsec-Scale Radio Jets, ed. J. A. Zensus & T. J. Pearson (Cambridge: Cambridge Univ. Press), 206
Witzel, A., Schalinski, C. J., Johnston, K., Biermann, P. L., Krichbaum, T. P., Hummel, C. A., & Eckart, A. 1988, A&A, 206, 245
Wrobel, J. M. 1987, in Superluminal Radio Sources, ed. J. A. Zensus & T. J. Pearson (Cambridge: Cambridge Univ. Press), 186
Wrobel, J. M., & Lind, K. R. 1990, ApJ, 348, 195
Wrobel, J. M., Pearson, T. J., Cohen, M. H., & Readhead, A. C. S. 1988, in IAU Symp. 129, The Impact of VLBI on Astrophysics and Geophysics, ed. M. J. Reid & J. M. Moran (Dordrecht: Reidel), 165
Zensus, J. A., Porcas, R. W., & Pauliny-Toth, I. I. K. 1984, A&A, 133, 27

© American Astronomical Society • Provided by the NASA Astrophysics Data System